Reducing Detrimental Defects for High-Performance Metal Halide Perovskite Solar Cells

Perovskite Solar Cells

International Edition: DOI: 10.1002/anie.201905521
German Edition: DOI: 10.1002/ange.201905521

Reducing Detrimental Defects for High-Performance Metal Halide Perovskite Solar Cells

Luis K. Ono, Shengzhong (Frank) Liu, and Yabing Qi**

Keywords:
electronic trap density · energy levels · passivation · perovskite solar cells · surface and bulk defects

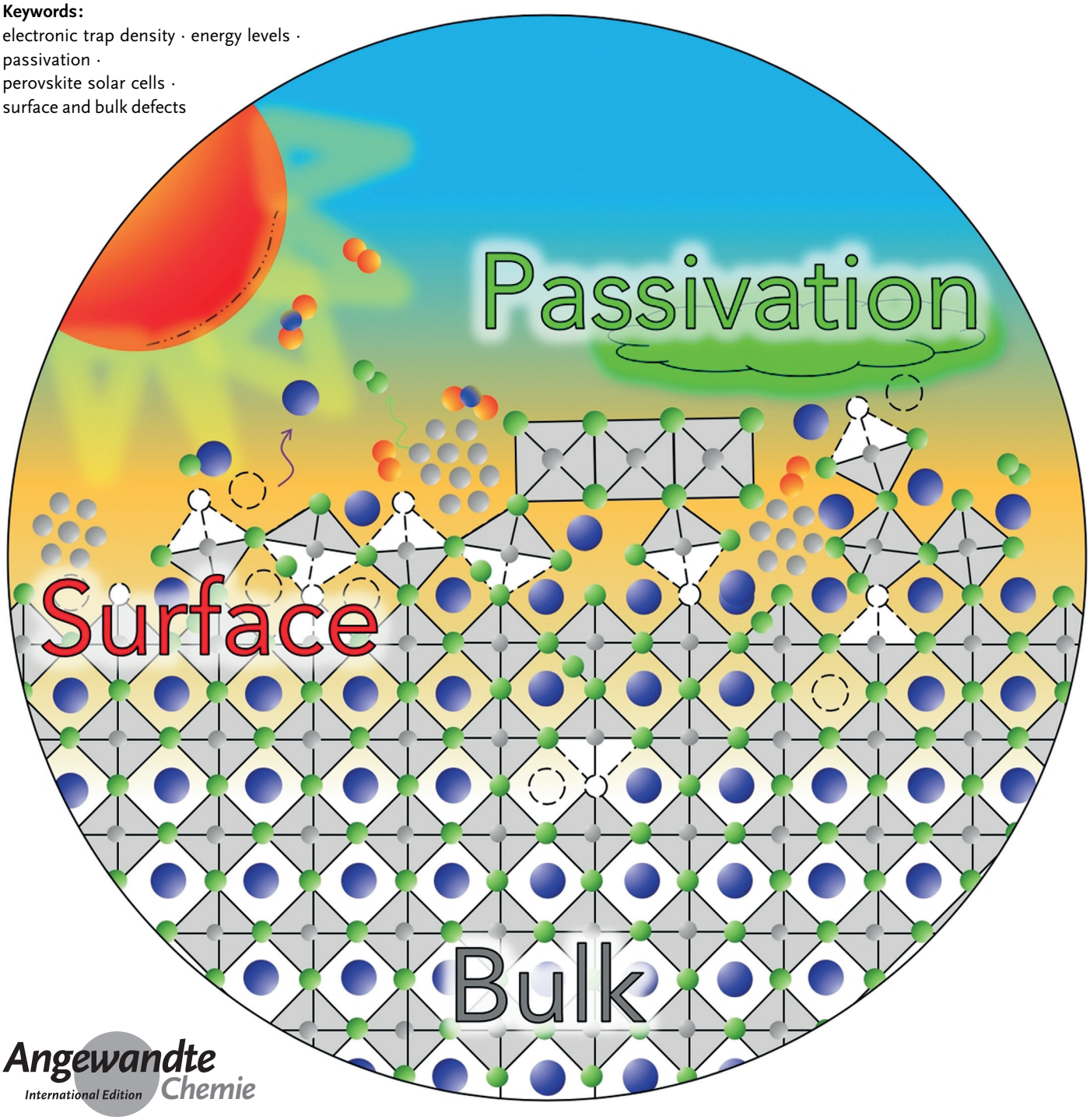

In several photovoltaic (PV) technologies, the presence of electronic defects within the semiconductor band gap limit the efficiency, reproducibility, as well as lifetime. Metal halide perovskites (MHPs) have drawn great attention because of their excellent photovoltaic properties that can be achieved even without a very strict film-growth control processing. Much has been done theoretically in describing the different point defects in MHPs. Herein, we discuss the experimental challenges in thoroughly characterizing the defects in MHPs such as, experimental assignment of the type of defects, defects densities, and the energy positions within the band gap induced by these defects. The second topic of this Review is passivation strategies. Based on a literature survey, the different types of defects that are important to consider and need to be minimized are examined. A complete fundamental understanding of defect nature in MHPs is needed to further improve their optoelectronic functionalities.

From the Contents

1. Introduction

Solar cells have emerged as a promising technology in the search for clean and sustainable energy sources. Research has been conducted to develop new emerging photovoltaic (PV) technologies[1] with desirable properties, such as being lightweight, flexible/bendable, low-cost and environmentally benign, which are not only alternative to current Si PV technology, but also can be useful in certain niche applications, such as building integrated photovoltaics (BIPVs), solar curtains, solar vehicles and airplanes, compact solar-charging systems. However, before commercialization can take off on a large-scale, these solar cells must be efficient, reproducible, and stable. Often a suitable PV material choice is based on selecting a semiconductor with a proper band gap, a high absorption coefficient, suitable charge-transport properties, and long-term stability.[2] The current PV market is still dominated by Si-wafer-based solar modules corresponding to a total of over 90% of the global market share.[2,3] The share of mono- and multi-crystalline silicon technology is around 32% and 61%, respectively. The market share of all thin-film technologies including CdTe (2.3%), copper indium gallium diselenide or CIGS (1.9%), and amorphous-Si (0.3%) amounts to only around 4.5% of total global solar module production.[6] When comparing these different commercialized PV technologies there is a general trend, that is, the solar cell performance is strongly dependent on the impurities and defects present in these semiconducting photovoltaic materials. In the literature, defects are often classified into two categories (i.e., shallow and deep) considering the practical device operation point of view.[7] A defect is regarded as shallow when the separation of its ground state energy level from the valence band (VB) or conduction band (CB) mobility edges is comparable to or lower than the thermal excitation energy k_BT (k_B is the Boltzmann constant and T is temperature) corresponding to room temperature (usual device operation temperature). Deep levels are states with the energy difference $E \gg k_BT$ from VB or CB edges in the mid-gap direction that can trap electrons or holes and decrease the overall carrier extraction/transport efficiency.[7,8] A major task in solar-cell fabrication has been devoted to the development of processing sequences that can minimize the deleterious impurities, point and cluster defects, and if unavoidable, how to passivate them. For instance, in Si technology, boron (electron acceptor) and phosphorous (electron donor) atoms are introduced to the Si crystal lattice to modify intrinsic Si properties to p-type and n-type semiconductors, respectively. These boron and phosphorous impurities or dopants (or extrinsic defects) in minute amounts lead to only shallow-level point defects in the Si band gap generating free carriers with desirable concentrations. Because shallow states are energy states formed near the VB or CB mobility edges, generally they are considered to be benign and offer a useful means to modulate semiconductor electronic properties. For example, although shallow defect states can also trap charge carriers, because of the relatively low activation energy required for these trapped charges to be excited to mobility edges, detrapping events occur at a relatively high rate, that is,

[*] Dr. L. K. Ono, Prof. Y. B. Qi
Energy Materials and Surface Sciences Unit (EMSSU), Okinawa Institute of Science and Technology Graduate University (OIST)
1919-1 Tancha, Onna-son, Kunigami-gun, Okinawa 904-0495 (Japan)
E-mail: Yabing.Qi@OIST.jp
Prof. S. Liu
Dalian National Laboratory for Clean Energy, iChEM, Dalian Institute of Chemical Physics, Chinese Academy of Sciences
457 Zhongshan Road, 116023 Dalian (China)
Prof. S. Liu
Key Laboratory of Applied Surface and Colloid Chemistry, Ministry of Education, Shaanxi Key Laboratory for Advanced Energy Devices, Shaanxi Engineering Lab for Advanced Energy Technology, School of Materials Science and Engineering, Shaanxi Normal University
Xi'an 710119 (China)
E-mail: liusz@snnu.edu.cn
Supporting information and the ORCID identification number(s) for the author(s) of this article can be found under: https://doi.org/10.1002/anie.201905521.

most of these trapped charge carriers can be thermally released to the bands before recombination can occur inducing minimal influences on charge-carrier transport.[9] On the other hand, intrinsic defects of low-coordinate Si atoms at the surface or dangling bonds introduce deep levels within the Si band gap that lead to decrease in the overall carrier transport efficiency. Furthermore, deep levels within the band gap can lead to electron–hole recombination (radiative, non-radiative, Auger recombination) that hinders the overall power conversion efficiency (PCE) in Si solar cells; therefore, deep levels show a detrimental effect on Si solar cells. Surface passivation by terminating the Si surface atoms with H atoms was demonstrated as an effective remedy to eliminate these deep-level states as a result of dangling bonds. In 2017, Kaneka Corporation applied the so-called passivating-contact solar cell technology setting the world's solar cell efficiency record of 26.6% with a designated area of 180.4 cm^2.[10] As well as the crystalline Si solar cells described above, polycrystalline solar cells that include Si, CdTe, CIGS, $Cu_2ZnSnSe_2$ (CZTSe), and Cu_2ZnSnS_2 (CZTS) materials offer the advantage of lower fabrication costs, but are also influenced by the quality of interfaces and densities of different types of defects such as point defects, stacking faults, twinning structures, dislocations, and grain boundaries.[11] Some defects, such as grain boundaries and interfaces, have very different electronic properties in these materials. For example, grain boundaries lead to harmful deep levels in Si and CdTe, but they do not produce deep levels in CIGS, CZTSe, and CZTS materials. This is why passivation is critical in Si and CdTe solar cells, while passivation is less important in CIGS and CZTS solar cells.[7a,11a] Organic semiconducting materials are more prone to the formation of trap states because of their disordered nature induced by the weak van der Waals interaction between molecules. As a consequence, these defects play a similar important role in the performance of organic solar cells.[12] Several Review articles provide insightful information about defects in Si, CdTe, CIGS, and organic based PV technologies.[7a,11a,13]

In this Review, we examine the current progress and challenges on the characterization of defects in metal halide perovskites (denoted as "perovskites" throughout the article). In the subsequent Sections, we provide our views on two topical subjects by analyzing published works on defects in metal halide perovskites. The first topic is the experimental challenges in identifying the different types of defects present in perovskites. Much has been done theoretically for proposing the presence of different types of point defects in perovskites. However, the probing of the different types of defects experimentally is rather challenging. On the basis of our survey shown in Table S1 in the Supporting Information and summarized in Figure 1a, we discuss the current progress for attaining a thorough characterization of these defects experimentally, such as 1) experimental assignment of the type of defects, 2) defects densities, and 3) the energy positions within the band gap induced by these defects. The second topic is based on a question if we are able to assign experimentally the different types of defects in perovskites based on the defect physics and coordination chemistry by the passivation strategies. Our survey shown in Table S2 and summarized in Figure 1b,c, provide a comprehensive list of the types of defects that are important to be considered and need to be minimized for solar cell applications. The recent work by Jiang et al.[14] employed the passivation strategy and obtained the certified record PCE of 23.3% and 23.7% in the National Renewable Energy Laboratory (NREL) chart.[1a] Acquiring a complete fundamental understanding of defects in perovskites is highly important to overcome technologically relevant issues for commercialization (efficiency, scaling-up, reproducibility, and stability).

2. Defects in Metal Halide Perovskites

Since the seminal works by Miyasaka et al.[15] and Park et al.,[16] perovskites have emerged as a promising class of materials for photovoltaic applications. Highly efficient perovskite solar cells are made from metal halide perovskites with an ABX_3 three-dimensional (3D) structure containing an organic/inorganic monovalent cation A^+ ($CH_3NH_3^+$, $CH(NH_2)_2^+$, or Cs^+), a divalent metal cation B^{2+} (Pb^{2+} or Sn^{2+}), and three halide anions X^- (I^-, Br^-, or Cl^-).[15c,17] Perovskites can be considered a soft ionic solid with semiconductor properties and a range of ubiquitous behaviors, such as hysteresis, ferroelectricity, ion migration, lattice vibrational properties influencing charge carrier transport.[11c,18] Similar to what has been found in inorganic and organic semiconductors, defects play an important role as well in the overall performance of perovskite-based solar cells. Notably, with simple and low-cost solution processing (e.g., spin-coating, blade coating), high PCEs are obtained for perovskite-based solar cells. This has been explained by a number of proposed models including: 1) the majority of defects formed have shallow defect energy positions within the band gap, 2) low density of deep traps (i.e., energy states close to

Luis K. Ono obtained his B.S. in Physics/Microelectronics from the University of São Paulo, Brazil. Later he joined the Department of Nuclear Engineering in Kyoto University, Japan, and the University of Central Florida, USA, where he obtained his M.S. and Ph.D., respectively. His current research focuses on the fundamental understanding and surface science aspects of perovskite solar cells.

Shengzhong Liu received his Ph.D. from Northwestern University (USA) in 1992. Following his postdoctoral research at Argonne National Laboratory (USA), he worked for various companies researching nanoscale materials, thin-film solar cells, laser processing, and diamond thin films. His invention of the semi-transparent photovoltaic module at BP Solar won an R&D 100 award in 2002. He is now a professor at Shaanxi Normal University and Dalian Institute of Chemical Physics, Chinese Academy of Sciences.

the middle of the band gap) and/or 3) their low capture cross section (i.e., interaction of traps with charges).[22] The different categories of defects illustrated in Figure 2 were previously proposed on the basis of both theoretical[23] and microscopy-based experimental reports[11b,19,24] (Figure 2 and Figure 4d,e). In perovskites with an ideal crystal structure (Figure 2a), each ion is located on its equilibrium site. However, in a real situation, because the crystal growth is fast and often a post-annealing treatment is required, the formation of a wide variety of structural defects is unavoidable.[11c,23c,24b,25] These imperfect lattice alignments can be of a short range due to point defects or impurity atoms/ions (Figure 2b–d,f or of a long range due to 1D dislocations, 2D grain boundaries, and 3D precipitates (Figure 2b,e,g.[11c,20,21,23c,24a,26] The generation of defects may take place not only during the perovskite synthesis processes, but also during the perovskite solar cell operation. For example, methylammonium lead iodide ($MAPbI_3$) undergoes photodecomposition and thermal degradation during solar cell operation.[5,27] Two reaction pathways were identified for these degradation processes (Figure 1c). One leads to the irreversible decomposition of organic volatile gas species ($CH_3I + NH_3$), and the other to reversible decomposition ($CH_3NH_2 + HI$). The $CH_3NH_2 + HI$ decomposition pathway is reversible because it can back react with PbI_2. The complete depletion of volatile organic components leads to a layer of PbI_2 on the perovskite film. Further decomposition of PbI_2 proceeds with reversible generation of I_2 and non-volatile metallic-Pb (Pb^0) under illumination or mild heating conditions (Figure 1c). Several X-ray photoelectron spectroscopy (XPS) studies report the existence of Pb^0.[32] Very likely these Pb^0 species exist at the surface or grain boundaries of perovskites, possibly as a core–shell structured cluster.[33] However, further studies are needed to provide more insights on the microscopic picture of how and where Pb^0 is located in the degraded perovskites. For example, as shown in Figure 3a,b, the possibility to form interstitial-Pb (Pb_i) was proposed, Pb_i would co-exist in the perovskite lattice and severely degrade device performance.[34] The other important type of defect is I_2. During degradation, I^- can be released from its lattice because I^- can be easily oxidized to I^0 (e.g., I_2 in Figure 1b,c).[5] The generated I_2 can further adsorb onto the surface or grain boundaries of perovskites leading to another type of defect center.[34a,b] In addition, it was further reported that I_2 vapor treatment may promote degradation in perovskite materials leading to increase in the density of defects.[4,35]

Yabing Qi received his B.S., M.Phil., and Ph.D. from Nanjing Univ., Hong Kong Univ. of Sci. and Tech., and UC Berkeley, respectively. He has published over 130 research articles and is the holder of 11 patents/patent applications. He is currently on the editorial board of JPhys Materials (IOP Publishing). His research interests include surface/interface sciences, perovskite solar cells, lithium ion batteries, organic electronics, energy materials and devices.

Point defects in $MAPbI_3$ were intensively studied in the past as a model material system. As comparison, theoretical sub-gap energy levels generated in formamidinium lead iodide ($FAPbI_3$),[36] $CsPbI_3$,[37] $CsPbBr_3$[38] were also reported. On the basis of theoretical calculations by Yan and coworkers 12 point defects are described for $MAPbI_3$: vacancies: MA (V_{MA}), Pb (V_{Pb}), and I (V_I); interstitials: MA (MA_i), Pb (Pb_i), and I (I_i); anti-site occupations: MA_{Pb}, MA_I, Pb_{MA}, Pb_I, I_{MA}, and I_{Pb} (Figure 3a).[23a,28] The theoretical predictions of defects that contribute as deep level states include I_{Pb}, I_{MA}, Pb_i, Pb_I, and Pb_{MA}.[11c,23c,39] However, these defects have high formation energies suggesting that they should not contribute to a high density of non-radiative recombination centers (Figure 3b).[18b,23a,28] The defects leading to shallow or intraband states (within VB and/or CB) have low formation energies, leading to high densities but are considered benign types of defect (Figure 3b,c). This is the most important feature of the so-called defect-tolerance in perovskites. The theoretical differences between the effects of point defects on the electronic properties of conventional defect-intolerant semiconductors, such as CdSe and GaAs, were previously described (Figure 3c).[18b,29,40] It is important to highlight that although shallow traps within the band gap lead to low occurrences of recombination processes, they lower the open-circuit voltage (V_{oc}).[41] V_{oc} in a solar cell is determined by the quasi-Fermi splitting of electrons and holes (E_{Fn}, E_{Fp}) under illumination. For instance, the E_{Fn} and E_{Fp} levels within the band gap are also affected by the occupation of the available electronic states by the photogenerated charge carriers, not only in the perovskite layer, but also in the adjacent selective contacts (Figure 3d,e).[30,31,42] Consider an initial scenario where the electron quasi-Fermi level of TiO_2, a commonly employed electron-transport layer (ETL) in perovskite solar cells, is aligned with the electron quasi-Fermi level of perovskite that has a low density of defects. In semiconductor materials, the shifting and pinning of the Fermi-level is a common phenomenon that is influenced by the defect density. Therefore, in the second scenario, where a particular perovskite has a high density of shallow traps at an energy of E_T below CB, the electron quasi-Fermi level of TiO_2 layer will be pinned to near this defect state E_T. Similarly, if a high density of shallow traps is present near the VB, the hole quasi-Fermi level of hole transporting layer (HTL) will also be pinned to the trap state energy. As a consequence, V_{oc}, which is given by the difference between the electron and hole quasi-Fermi levels under illumination, will decrease in solar cells with perovskite materials with a high density of shallow traps. In the presence of shallow traps a new quasi-Fermi level pinning will take place dictating the energy level alignments at the ETL/perovskite/HTL interfaces.[30,31,42] Therefore, shallow traps near the CB and VB with a narrow distributed density of states (DOS) is desirable to raise the quasi-Fermi level (E_{Fn}) of photogenerated electrons and minimize V_{oc} losses (ΔV_{oc}).

A summary of attempts to verify experimentally the theoretical predictions (Figure 3a) of trap state energy levels and trap densities in perovskites are shown in Table S1 and

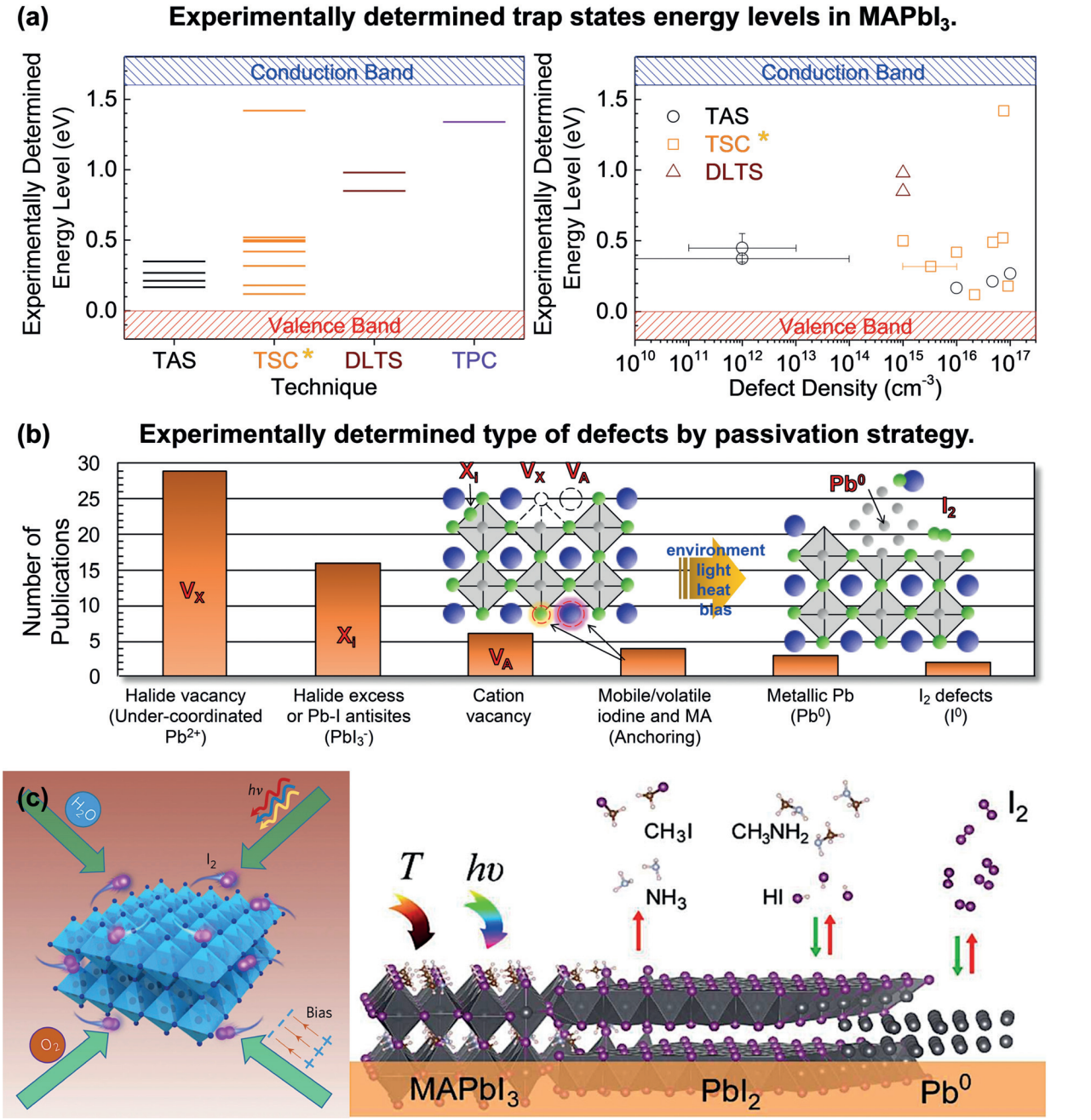

Figure 1. a) Left: Experimentally determined energy levels associated with defects in $MAPbI_3$ and determined by the different techniques of TAS = thermal admittance spectroscopy, TSC = thermally stimulated current, DLTS = deep-level transient spectroscopy, and TPC = transient photocapacitance. Right: Experimentally determined energy levels of defects in $MAPbI_3$ associated with their defect density. *TSC measurements provide only activation energies and cannot determine whether these activation energies are referenced to the valence band or conduction band. In the plots, the defect energy values were referenced to the valence band minimum. b) Histogram indicating the number of publication on the experimentally assigned types of defects in perovskites employing passivation strategies. c) Left: During solar-cell operation multiple factors, such as H_2O and O_2 in ambient air, light, heat, and bias voltage can lead to degradation and further generation of defects in perovskites. Right: illustration of the proposed microscopic picture of the different defects that can be generated during degradation of perovskite materials. Note that for this process, the overall charge neutrality should be conserved. Left image was reprinted with permission from Ref. [4]. Copyright 2016 Springer Nature Publishing AG. Right image was reprinted with permission from Ref. [5]. Copyright 2018 The Royal Society of Chemistry.

depicted in Figure 1a (for the $MAPbI_3$ case). Several techniques previously developed to understand the features of defects (energy levels and densities) in inorganic semiconductors were applied also in perovskites.[11c,43] These techniques include temperature-dependent charge space limited current (SCLC), thermal admittance spectroscopy (TAS), deep-level transient spectroscopy (DLTS), Laplace current DLTS (I-DLTS), steady-state photoluminescence (SSPL), time-resolved photoluminescence (TRPL), PL mapping,[44] time-resolved microwave conductivity (TRMC),

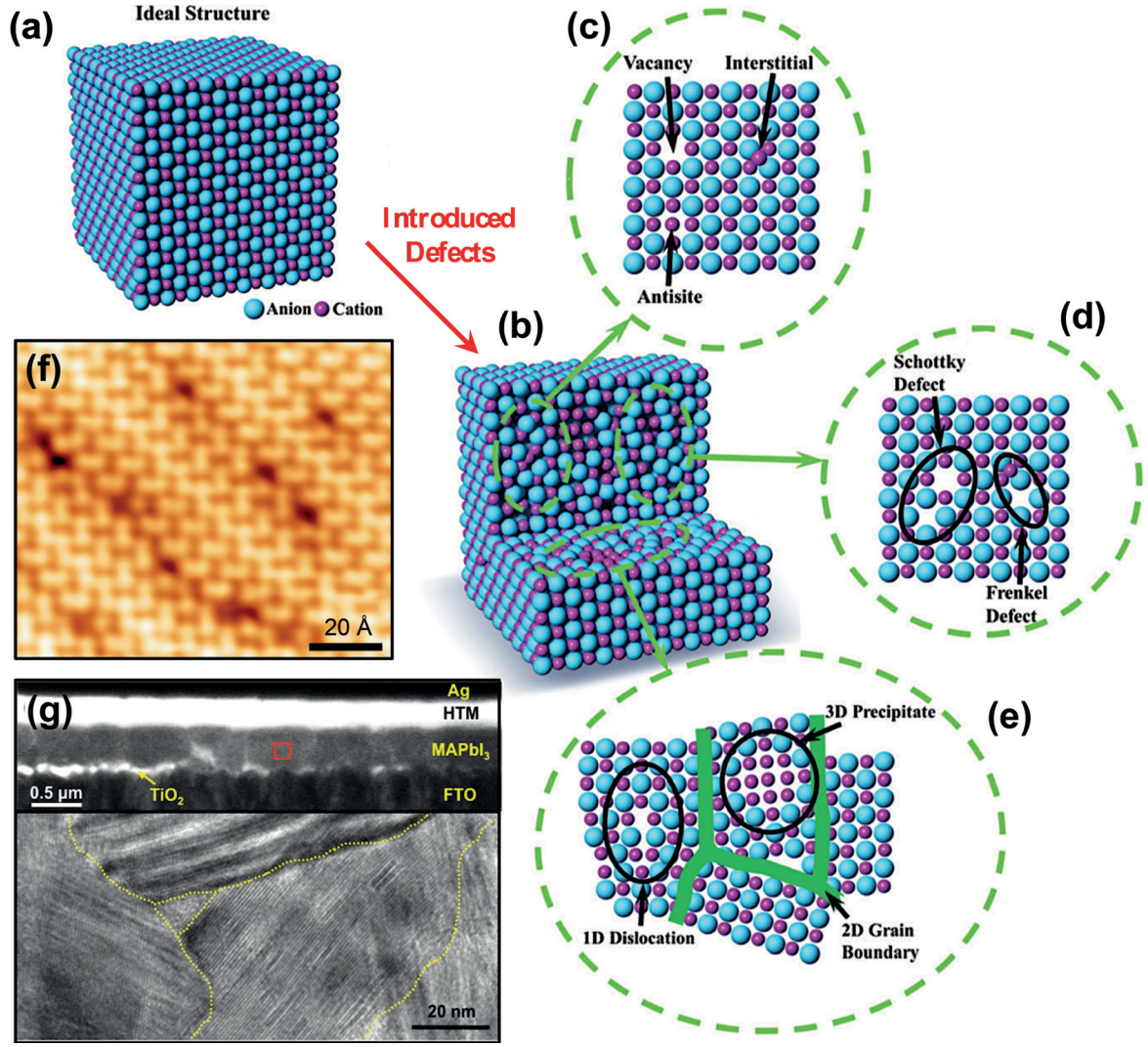

Figure 2. Illustration of a) stoichiometric crystal structure (or perfect lattice structure) of a semiconductor without defects and b) after defects are generated, for example, during crystal growth and/or post-treatment processes. c)–e) The microscopic configurations for these types of defects in a perovskite crystal lattice. Panels (a)–(e) were reprinted with permission from Ref. [11c]. Copyright 2018 The Royal Society of Chemistry. f) Point/cluster defects and dislocations visualized by STM in $MAPbBr_3$ crystal (9.2×10.3 nm^2). Reprinted with permission from Ref. [19]. Copyright 2015 American Chemical Society. g) Top: Cross-sectional TEM image of a planar $MAPbI_3$ polycrystalline film and, bottom: high-resolution TEM inside a grain. Apparent sub-grain features are indicated by yellow dashed lines. Top: Reprinted with permission from Ref. [20]. Copyright 2015 WILEY-VCH Verlag GmbH & Co. KGaA, Weinheim. Bottom: Reprinted with permission from Ref. [21]. Copyright 2015 The Royal Society of Chemistry. Note: top and bottom images in (g) are not from the same sample.

thermally stimulated current (TSC), capacitance-frequency at different temperatures (C-f), transient photocapacitance (TPC), surface photovoltage (SPV) spectroscopy,[45] time-resolved spectroscopies such as transient absorption and reflection techniques,[46] ultraviolet photoemission spectroscopy (UPS),[42b,47] scanning tunneling microscopy (STM).[19,25d,48] Comprehensive Reviews describing the working principles of techniques above and summarizing advantages and disadvantages can be found in Refs. [11c,43]. On the basis of Table S1, it is noticed that 1) all the techniques above provide an ensemble averaged signal over the delimited electrode size or spot size of excitation probing light beam; 2) there is a strong influence from the measurement environmental conditions; 3) none of the techniques can provide the experimental assignment of a defect energy to a certain type of defect. Regarding (1), surface and bulk defects show different properties (Figure 4a) and the instrument measurement properties (e.g., surface and/or bulk trap states, sensitivity, probing depth) need be considered.[49] Furthermore, in addition to single defects, larger and complex defect types, such as dislocations, grain boundaries, and cluster precipitates (Figure 2e,g) are expected to be generated during the different fabrication conditions (e.g., precursor ratios and concentrations, solvents, impurities, environment, temperature).[50] Although the number of experimental observations is still scarce, sub-grain twinning domains in perovskites have been recently reported.[11b,24c–f] On the basis of high-resolution transmission electron microscopy (HR-TEM), Kim et al.[11b] revealed that the tetragonal and cubic phases co-exist at room temperature (RT) in

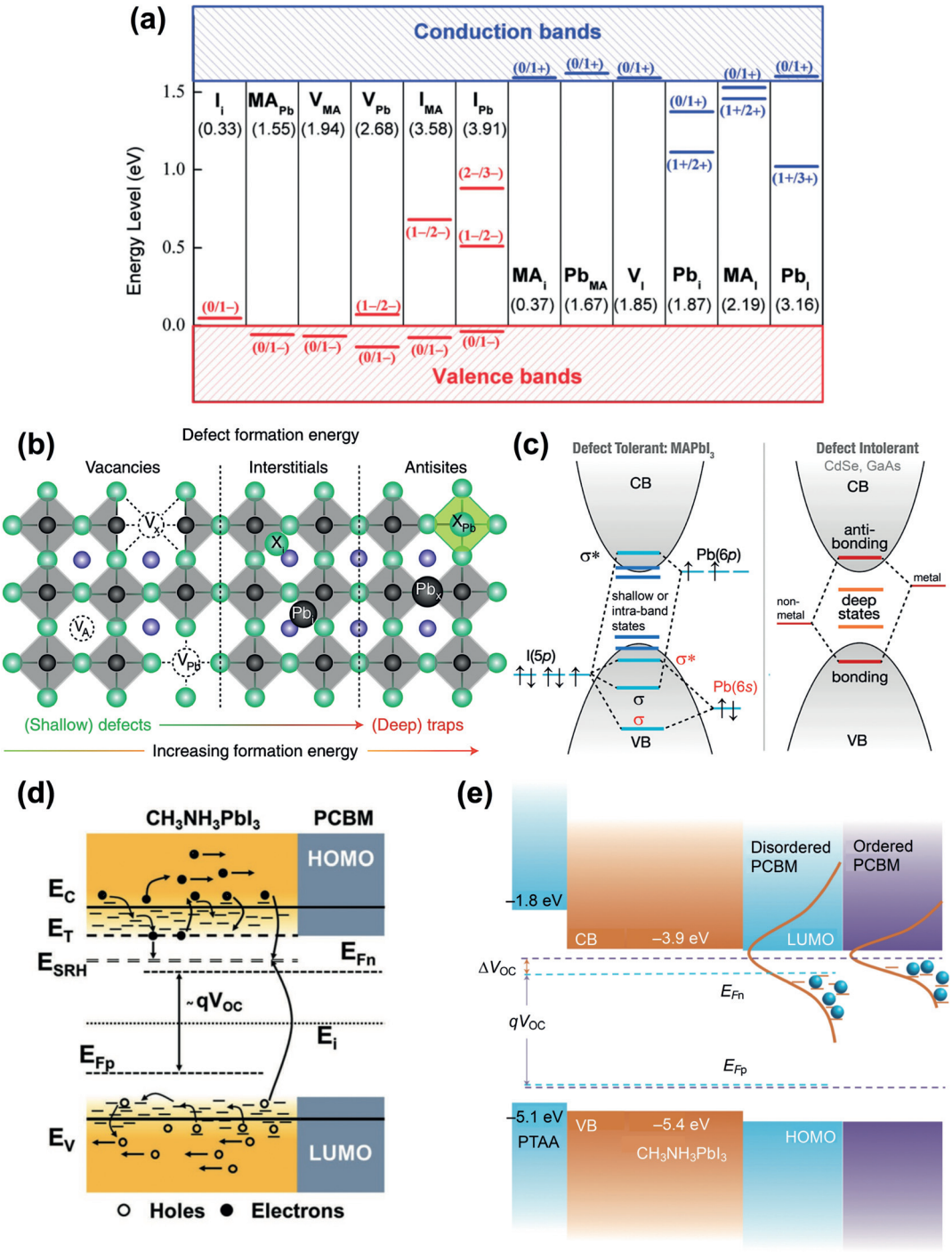

Figure 3. a) Calculated energy states of point defects in $MAPbI_3$. The formation energies of neutral defects are shown in parenthesis. The acceptor (red) and donor (blue) type defects are ordered by the formation energies. Reprinted with permission from Ref. [28]. Copyright 2014 WILEY-VCH Verlag GmbH & Co. KGaA, Weinheim. b) Illustration of point defects in perovskites, including vacancies, interstitial and anti-site atoms, in order of increasing formation energy that corresponds to decreasing probability of occurrence. Reprinted with permission from Ref. [18b]. Copyright 2018 Springer Nature Publishing AG. c) Schematic illustration of electronic structures that are defect-tolerant (e.g., $MAPbI_3$) and defect-intolerant (e.g., CdSe, GaAs, and InP). Reprinted with permission from Ref. [29]. Copyright 2017 American Chemical Society. d) Schematic illustration showing how a high density of shallow trap states in perovskites and/or e) energy disorder (e.g., induced by structural disordered PCBM layer) influence the device V_{oc}: A wide distribution of traps reduces the quasi-Fermi level of photogenerated electrons and holes (E_{Fn}, E_{Fp}) and thus reduce device V_{oc}. Panel (d) was reprinted with permission from Ref. [30]. Copyright 2017 WILEY-VCH Verlag GmbH & Co. KGaA, Weinheim. Panel (e) was reprinted with permission from Ref. [31]. Copyright 2016 Springer Nature Publishing AG.

$MAPbI_3$ films. Triple (tetragonal/cubic/tetragonal) and double (tetragonal/cubic) layers of stacking sequences are formed spontaneously. As a consequence, the microstructural domain-walls within the stacking layers were suggested to

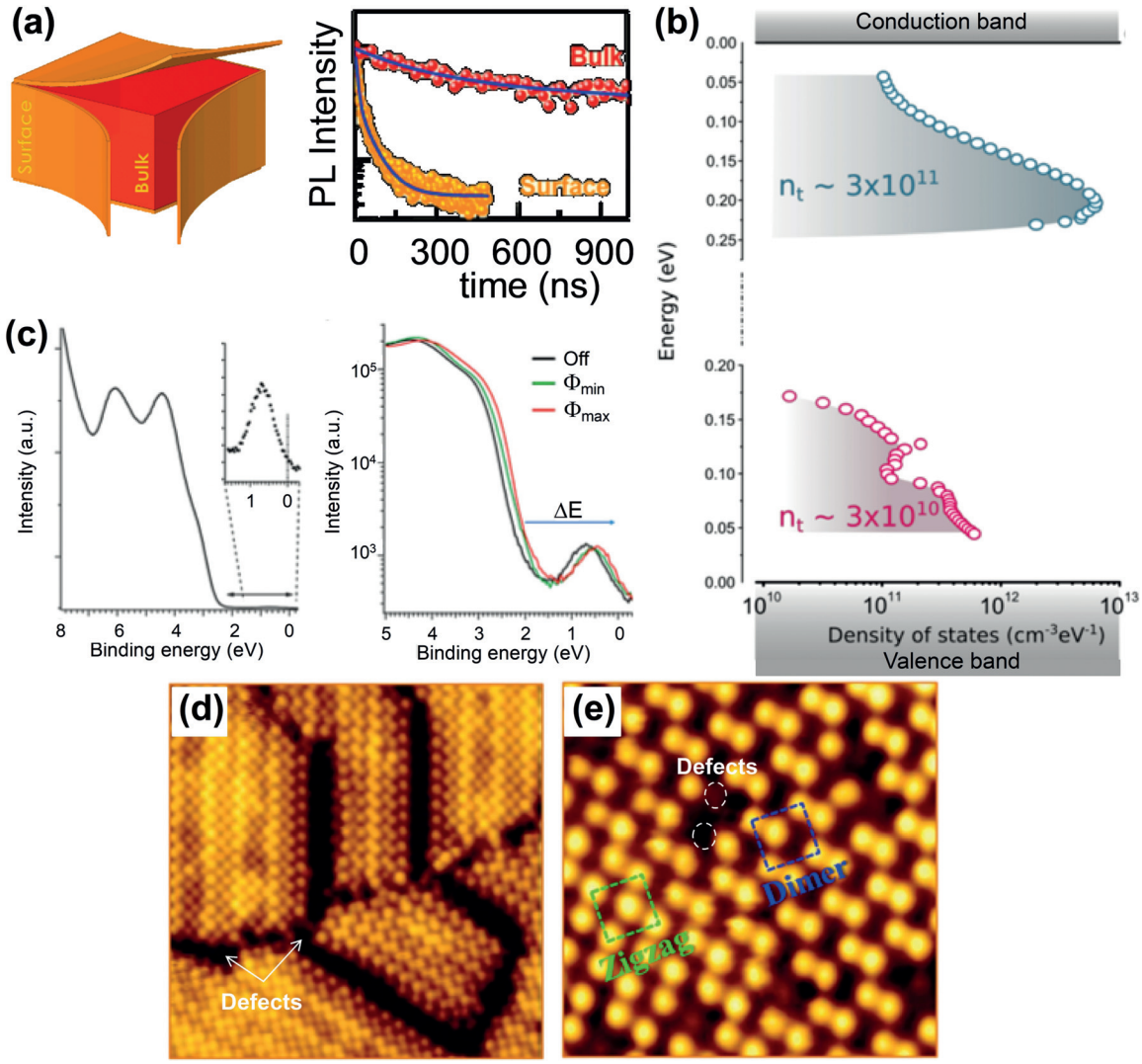

Figure 4. a) highlighting the importance of different optical and electronic properties at the surface compared to the bulk of perovskite crystals. Reprinted with permission from Ref. [49a]. Copyright 2017 American Chemical Society. b) Density of trap states of $MAPbI_3$ single crystals within the band gap extracted from the temperature dependent SCLC technique. Reprinted with permission from Ref. [43d]. Copyright 2016 WILEY-VCH Verlag GmbH & Co. KGaA, Weinheim. c) UPS with $h\nu = 21.22$ eV on in situ cleaved $MAPbBr_3$ single-crystal surface (left) and semi-log plot under 1.5 mW (green line) and 4.5 mW (red line) white illumination. Reprinted with permission from Ref. [47b]. Copyright 2017 Springer Nature Publishing AG. d),e) High-resolution STM images acquired on vacuum co-deposited $MAPbI_3$ polycrystalline films with a coverage of 4.5 ML (ML = monolayer) showing grain-boundaries (d) and defects as dark protrusions (e) (19×19 nm^2, 6.9×6.9 nm^2; $V = 1.5$ V, 1.2 V; I = 150 pA, 100 pA). Reprinted with permission from Ref. [48f]. Copyright 2017, Elsevier Ltd.

influence charge carrier transport properties.[11b,40,51] Therefore, it is imperative to carefully examine the relationship between microscopic structural information and their corresponding energy levels.[19,24b,25d,48b,c,e,f]

Point (2) relates to the sample measurement conditions (i.e., physisorption and/or chemisorption of gases such as O_2 and H_2O, temperature, light intensity), which has been evidenced to show significant influences on the characterization of defects.[43a,49b,52] For example, Gordillo et al.[43a] employed the TSC technique to probe the influences of oxygen adsorption on the energy levels of traps and the density of trap centers. Analysis of TSC curves obtained from measurements performed inside a vacuum chamber under different oxygen partial pressures, revealed the presence of trap centers whose activation energies are affected by the oxygen concentration. Similar studies show that not only O_2, but also H_2O and CH_3I vapors have influences on optoelectronic properties of perovskites.[49b,53] Furthermore, a deep understanding of working principles for these advanced analytical tools as well as the expertise to carry out related data analysis and interpretation are vital for obtaining reliable data and accurate interpretation, which could be the reason that only a few groups utilized these advanced analytical tools in perovskite research and relatively little data exists in some cases. For example, one needs to understand various types of unintentional artefacts caused by the probing (excitation) sources in analytical tools (e.g., ToF-SIMS or XPS) and devise proper procedures to minimize these artefacts to obtain reliable data.

Regarding Point (3), the ensemble average measurements do provide the overall averaged energy levels and densities of trap centers. For example, SCLC has been widely employed for the determination of trap densities in $MAPbI_3$,[43d,54] $MAPbBr_3$,[54a–c] $FAPbI_3$,[54e,55] and $FAPbBr_3$[55c] crystals.[11c] Values for defect densities range from 10^9 to $10^{10}\,cm^{-3}$ for solution-grown perovskite crystals; the employment of the temperature dependent SCLC technique allows the determination of trap energy levels (Figure 4b).[43d] For comparison, polycrystalline $MAPbI_3$ thin films have shown a larger density of defects on the order of $10^{16}\,cm^{-3}$.[11c,24b] TAS and DLTS provide the energy level positions of defects within the band gap as well as trap densities. In several studies employing TAS, it is proposed that perovskites have a p-type semiconductor nature.[56] In this scenario, it has been shown that the defect activation energy corresponds approximately to the depth of defect state energy level relative to the VB of the perovskite.[56] All these techniques have the major limitation that they are not able to visualize in real space or provide direct assignments of defect types.[19,24b,25d,48b,c,e,f] In this sense, photoelectron spectroscopy combining UPS and XPS may be a viable way to determine the defect energy levels and densities as well as the nature of defects (Figure 4c).[12,47a,57] For example, Zu et al.[42a,b] employed UPS/XPS to probe the surface trap states in $MAPbI_{3-x}Cl_x$ perovskites and reported that they consisted mainly of elemental (reduced) lead (Pb^0). These Pb^0 defects act as donor levels pinning the Fermi level at the surfaces of perovskites leading to n-type semiconductor character. The presence of uncoordinated Pb sites in perovskites have been confirmed by others.[5,32b] Although UPS/XPS were demonstrated as effective tools to probe and characterize defects, they cannot provide vital real space visualization of the features, and therefore cannot relate the observation of energetic features in UPS/XPS spectra to their microscopic origins (see for example Figure 4c). It is likely that local properties on a much smaller scale, at the micrometer or even nanometer scale, are the key to settling many existing controversial issues in perovskite materials and solar cells.[19,24b,25d] Since 2014, scanning tunneling microscopy and spectroscopy (STM/STS) have been used to investigate and correlate the structural and electronic properties at the atomic level.[19,25d,48a,b,58] STM and STS can be used to visualize in real space defects at the atomic level and characterize their electronic properties on the perovskite surfaces (Figure 2f and Figure 4d,e). There has been substantial progress in investigating intensively the real-space visualization of atomic structures and electronic properties of non-stoichiometric (i.e., defects) in perovskite surfaces by STM/STS.[19,24b,25d,48b,c,e,f] On the basis of DFT calculations,[48a] the dark protrusions observed in Figure 2f were tentatively assigned to Br and/or Br-MA vacancies, which however need to be confirmed with further studies.[19,24b,25d] She et al.[48c,f] and Cai et al.[48g] provided the STM images on vacuum co-evaporated $MAPbI_3$ polycrystalline films (Figure 4d,e) in which similar dark protrusions were observed most likely corresponding to the I and/or I-MA vacancies.[48a]

In this Section, we have provided a comprehensive summary (Table S1 and Figure 1a) of the experimental efforts to characterize and determine the energy level of trap states induced by crystal defects as well as their respective trap densities. These trap states energy levels and their densities affect the Fermi level, which leads to p- or n-type semiconductor behaviors with technological implications. These defect states are also responsible for carrier trapping and non-radiative recombination dynamics hindering efficient solar cell operation. Despite the scarce number of studies to characterize defects (Table S1 and Figure 1a), it is worth noting that a high density of defects ranging from $10^{15}\,cm^{-3}$ to $10^{17}\,cm^{-3}$ are reported (Figure 1a). These defects penetrate relatively deep within the band gap and sufficiently far away from the VB or CB mobility edges ($E_T \gg \approx 25$ meV).[56b] Figure 1a shows the energy levels of trap states and respective trap densities based on the reported studies employing multiple techniques (TAS, DLTS, TSC, TPC). However, the experimental determination of the type and microscopic nature of defects is currently a particular challenging task for perovskite materials, which is in sharp contrast to the well-established understanding about various types of defects in silicon.[59] In the next Section, we aim at analyzing whether it is possible to identify the type of defects based on their coordination chemistry as explored by using the passivation strategy.

3. Defect Passivation in Metal Halide Perovskites

In Si-technology, passivation of dangling bonds is often achieved by the formation of Si–H, Si–N, and Si–O, covalent bonds. In particular, H-passivation in Si can diffuse into bulk and heal bulk shallow traps.[60]

Similarly, several strategies of surface passivation have been proposed for thin-film solar cell technologies of CIGS and CdTe that resulted in enhancements in their performance.[13a,61] On the basis of such knowledge, several passivation chemistry strategies were also proposed in perovskite materials. The ionic nature of perovskites requires different defect passivation strategies from covalent-bonding semiconductors because the defects in perovskites are charged, either positively (e.g., a halide ion vacancy leading to under-coordinated Pb^{2+}) or negatively (e.g., a MA^+ cation vacancy and PbI_3^- anti-site defect); however, the overall charge neutrality should be conserved.[62] Several comprehensive Review articles summarize recent progress on this topic.[11c,43c,63] In this Section, on the basis of reported work on strategic coordination chemistry used to reduce the density of defects in perovskites, we aim at analyzing the rationale of the various physico-chemical (e.g., passivation by Lewis base and Lewis acid molecules) approaches. In the previous Section, we surveyed the literature on experimentally characterizing the defects in perovskites (Figure 1a and Table S1), and pointed out that although the analytical tools employed in all these studies provide quantitative analyses of energy levels of trap states and respective trap densities, usually they are not able to experimentally determine the microscopic origin of these defects. In some cases, such assignments are attempted on the basis of a comparison between experimental data with theoretical calculations. In this Section, we focus on this central question, that is, how the different types of defects in

perovskites can be experimentally probed by devising proper passivation strategies. Often analytical tools, such as Fourier transform infrared (FTIR), XPS, time-of-flight secondary ion mass spectrometry (TOF-SIMS), Raman, and energy-dispersive X-ray (EDX) spectroscopy, are employed to study the coordination chemistry between the passivating molecule and defects in perovskites. As summarized in Table S2, several small-molecules have been demonstrated to passivate effectively defects present at the grain boundaries and on the surface of perovskite films. Two approaches of post-passivation treatment and additives added in the perovskite precursor solution were proposed as defect engineering approaches.[43c,63a] On the basis of Table S2 and Figure 1b, a central discussion of the types of defects and their passivation strategies are focused on the 1) halide vacancies (e.g., Cl^-, Br^-, I^-) leading to exposure of under-coordinated positively charged Pb^{2+} atoms,[63d,64,66] 2) negatively charged Pb-I anti-sites (PbI_3^-) or halide-excess,[65,67] 3) cation vacancies (e.g., Cs^+, MA^+), 4) metallic lead (Pb^0) surface terminated,[5,32a,34a,68] 5) mobile or volatile I^- anion and MA^+ cations,[5,65,69] and 6) I^0 (I_2) defects.[4,5,34a]

The surface under-coordinated Pb^{2+} (Figure 1b and Figure 5a–c) is the main source of trap states and several chemicals have been proposed to heal this particular type of defect. A selection of organic molecules containing Lewis base functional groups, such as pyridine,[64,70] thiophene,[64] thiourea,[71] 6,6,12,12-tetrakis(4-hex-ylphenyl)-indacenobis-(dithieno[3,2-b;2,3-d]thiophene) end-capped with 1,1-dicyanomethylene-3-indanone units with 0 to 2 fluorine substituents (INIC),[72] perylene diimide and dithienothiophene (PPDIDTT),[73] benzodithiophene and diketopyrrolopyrrole with linear alkylthio substituents (BDTS-2DPP),[74] 1,3,4-thiadiazolidine-2,5-dithione (TDZDT),[75] organic semiconducting non-fullerene acceptor molecule named IT-M,[76] 3,9-bis(2-meth- ylene-(3-(1,1-dicyanomethylene)-indanone))-5,5,11,11-tetrakis(5-hexylthienyl)-dithieno[2,3-d:2′,3′-d′]-s-indaceno[1,2-b:5,6-b′] dithiophene (ITIC-Th),[77] 2-(6-bromo-1,3-dioxo-1H-benzo[de]isoquinolin-2(3H)-yl)ethan-1-ammonium iodide (2-NAM),[78] and others[79] were employed. Lewis base can coordinate with Pb^{2+} through lone pair electrons neutralizing its positive charge leading to subsequent annihilation of electronic trap states. These passivation treatments often result in significant enhancement in photoluminescence quantum yield (PLQY) and longer-lived excited charge carrier lifetime in perovskites often interpreted as decrease of non-radiative recombination centers. In addition, a blue shift in the PL peak after the perovskite passivation is indicative of suppressed radiative recombination between charge traps.[76]

Nenon et al.[63d] proposed that because the under-coordinated Pb^{2+} shows relatively a soft Lewis acid nature, the hardness or softness of the Lewis base of passivating molecules plays a role in efficacy of passivation (Figure 5a–c). Passivating molecules with harder species (e.g., alkylcarboxylates, carbonates, and nitrates) are ineffective passivating ligands, while softer species (e.g., alkylphosphonates, fluorinated carboxylates, and sulfonates) were found to be effective in passivating under-coordinated Pb^{2+}.[63d] Although the reported passivating molecules are effective in suppressing the surface dominated charge traps, the chemical stability of these molecules is an important consideration. It is desirable that the passivating molecules are strongly anchored to the defect sites in perovskites. However, it has been reported that some passivating molecules can be removed by subsequent washing with common solvent (e.g., isopropanol,[83] chlorobenzene[84]). Zhang et al.[84] showed that the use of 2-mercaptopyridine (2-MP), a bidentate molecule, increases anchoring strength improving passivation efficacy and stability simultaneously. Compared to monodentate counterparts of pyridine and *p*-toluenethiol where the coordination with Pb^{2+} can be easily broken because of low binding strength, the passivation by 2-MP on $CH_3NH_3PbI_3$ films led to enhanced tolerance to chlorobenzene washing and vacuum heating.[84]

Another category of defects discussed in literature are associated with the negatively charged Pb-I anti-sites (PbI_3^-) and under-coordinated halide ions (Figure 5d). Lewis acids, such as phenyl-C61-butyric acid methyl ester (PCBM),[67,85] $A_{10}C_{60}$,[86] iodopentafluorobenzene (IPFB),[65] KI,[87] $ZnCl_2$,[88] were proposed to effectively passivate these sites. The coordination chemistry is based on the acid–base theory and it was proposed that the negatively charged PbI_3^- anti-sites and under-coordinated halide ions donate electrons to Lewis acids leading to passivation. So far, most of these passivation molecules can only passivate one type of defect. Recently, it has been pointed out that the charge neutrality consideration is important when considering the passivation of charged defects in perovskites.[62a,66] A trend in the passivation strategy exists based on employing passivating molecules with the dual function of Lewis base and Lewis acid or two additives leading to synergistic effects of passivating both type of positively and negatively charged defects simultaneously (Figure 5b,c).[56b,62,66,69a,80,89] Zheng et al.[66] introduced a sulfonic zwitterion, 3-(decyldimethylammonio)-propane-sulfonate inner salt (DPSI), which contains both a positively charged quaternary ammonium group and a negatively charged sulfonic group. On the basis of FTIR spectroscopy, the coordination of sulfonic group (S=O) of DPSI to $MAPbI_3$ by the donation of their lone unpaired electron to the empty orbitals of Pb^{2+} was proposed. Alternatively, Zhang et al.[62c] reported on employing bis-PCBM as the Lewis acid and *N*-(4-bromophenyl)thiourea (BrPh-ThR) as the Lewis base. The combination of these two passivating molecules shows the synergistic effect of passivating both the positively charged under-coordinated Pb^{2+} and negatively charged PbX_3^- anti-sites defects. Bi et al.[89f] described on the multifunctional molecular modulator of 3-(5-mercapto-1*H*-tetrazol-1-yl)benzenaminium iodide, composed of hydrophobic heteroaromatic cores functionalized by ammonium ($-NH_3^+$) and thiol groups (-SH). On the basis of combined experimental techniques of FTIR, NMR, XPS, and XRD, it was rationalized that 1) the ammonium group effectively coordinates with A^+ cation vacancy defects, while 2) the thiol group coordinates with under-coordinated Pb^{2+} defects. Furthermore, 3) the unique tautomeric form of this molecule exposes the additional hydrogen bonds enhancing the interaction with the perovskite surface (via A^+ cations). 4) The fourth functionality is associated with the enlargement in grain size induced by the thiol groups. The growth of monolithic-type and/or

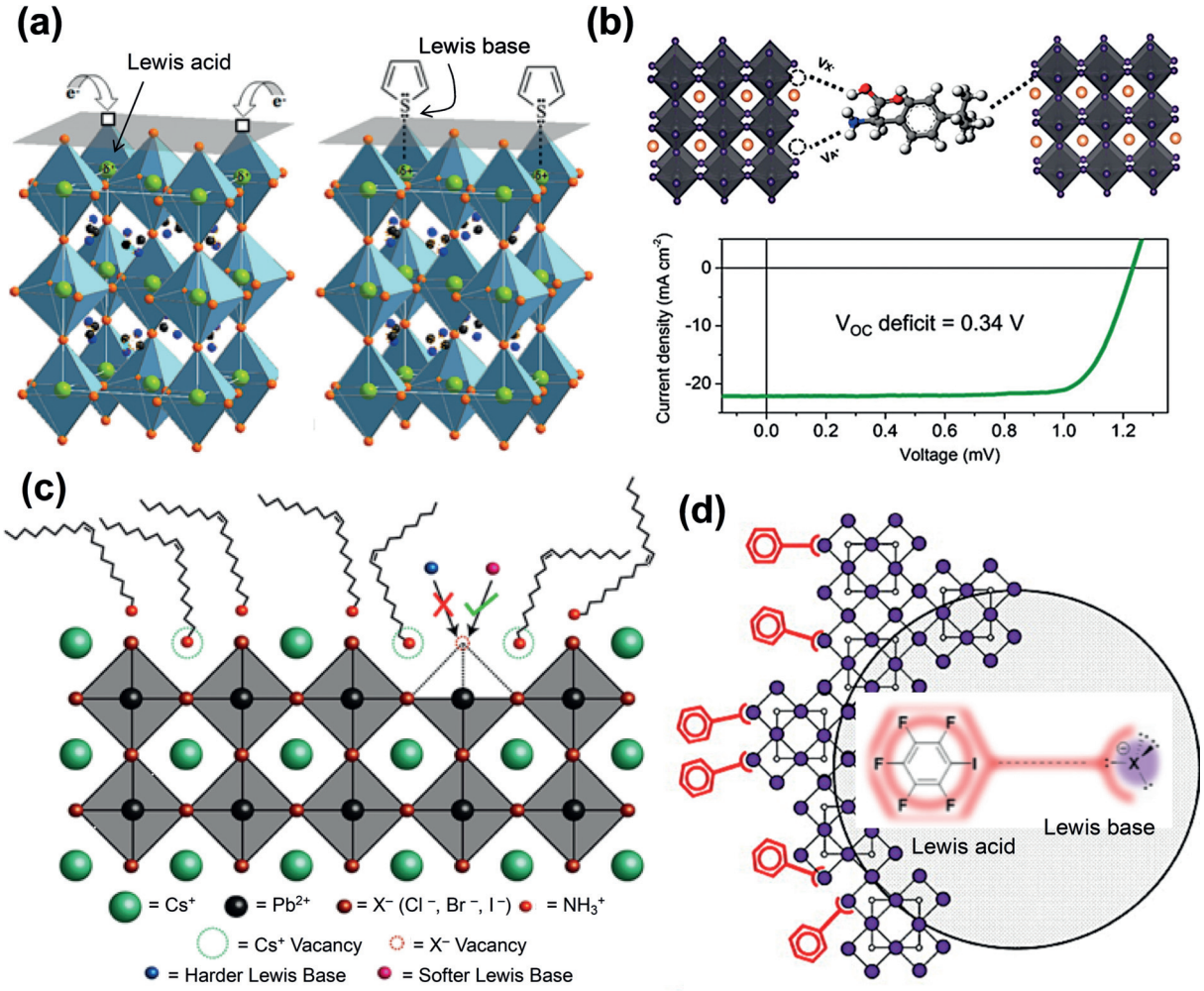

Figure 5. a) Schematic illustration showing the halide vacancy exposing the underlying under-coordinated Pb^{2+} that has the soft Lewis acid nature. The under-coordinated Pb^{2+} acts also as electron traps deteriorating charge transport efficiency. Thiophene (or pyridine) molecules coordinate with Pb^{2+} by donating electron density, neutralizing the excess positive charge. Reprinted with permission from Ref. [64]. Copyright 2014 American Chemical Society. b) Schematic illustration of D-4-*tert*-butylphenylalanin (D4TBP) mediated $MAPbI_3$ perovskite defect passivation and halide anchoring at grain boundaries and film surfaces. Reprinted with permission from Ref. [62b]. Copyright 2019 American Chemical Society. c) Schematic illustration of Cs and halide vacancies surface terminated by CsX (X = Cl^-, Br^-, I^-) confirmed by experimental results employing passivation strategy. Halide vacancies lead to under-coordinated Pb^{2+}, which can be either left unpassivated or passivated, depending on the hardness or softness of the Lewis base that coordinates with Pb^{2+} site. Reprinted with permission from Ref. [63d]. Copyright 2018 American Chemical Society. d) The Lewis acid passivation strategy for the under-coordinated iodide? ions at the perovskite surface using iodopentafluorobenzene (IPFB) by the supramolecular halogen bond complexation. Reprinted with permission from Ref. [65]. Copyright 2014 American Chemical Society.

large perovskite grains in polycrystalline films is a widely employed strategy to reduce detrimental defects.[7a,54e,89f,90] Although several groups have reported that amino-functionalized groups are efficient for passivating under-coordinated PbI_6 octahedra (Table S2), Xu et al.[91] demonstrated that the strength of interaction of hydrogen bonds with organic cations (FA^+ in $FAPbI_3$) could decrease the passivation efficiency of amine groups with under-coordinated Pb^{2+} defects (or V_I). To demonstrate this effect, two similar amino-functionalized molecules of 2,2′-(ethylenedioxy)diethylamine (EDEA) and hexa-methylenediamine (HMDA) were first investigated, which have an identical length of alkyl chains; the difference is that EDEA has two additional O atoms within the chain (Figure 6a). Combined techniques of FTIR and NMR together with DFT reveal that the presence of O (electron-rich) atoms in the alkyl chain withdraws electrons from N atoms towards O atoms. This property weakens the electron-donating ability of the amino groups, reducing the hydrogen-bonding ability with FA^+ cations ($E_{ads,P} = -1.42$ eV; Figure 6a). As comparison, HMDA that contains no O atoms in the alkyl chain leads to a stronger adsorption energy with FA^+ on a defect-free surface ($E_{ads,P} = -1.66$ eV). For the $FAPbI_3$ surface with V_I defects, the additional interaction energies of EDEA and HMDA with iodide vacancy defects were calculated to be $E_{ads,V=}-1.65$ eV and -1.21 eV, respectively. This means that the presence of O atoms (that weakens the hydrogen-bonding strength) is preferred for enhancing the passivation effect on perovskite surfaces with V_I. This is in

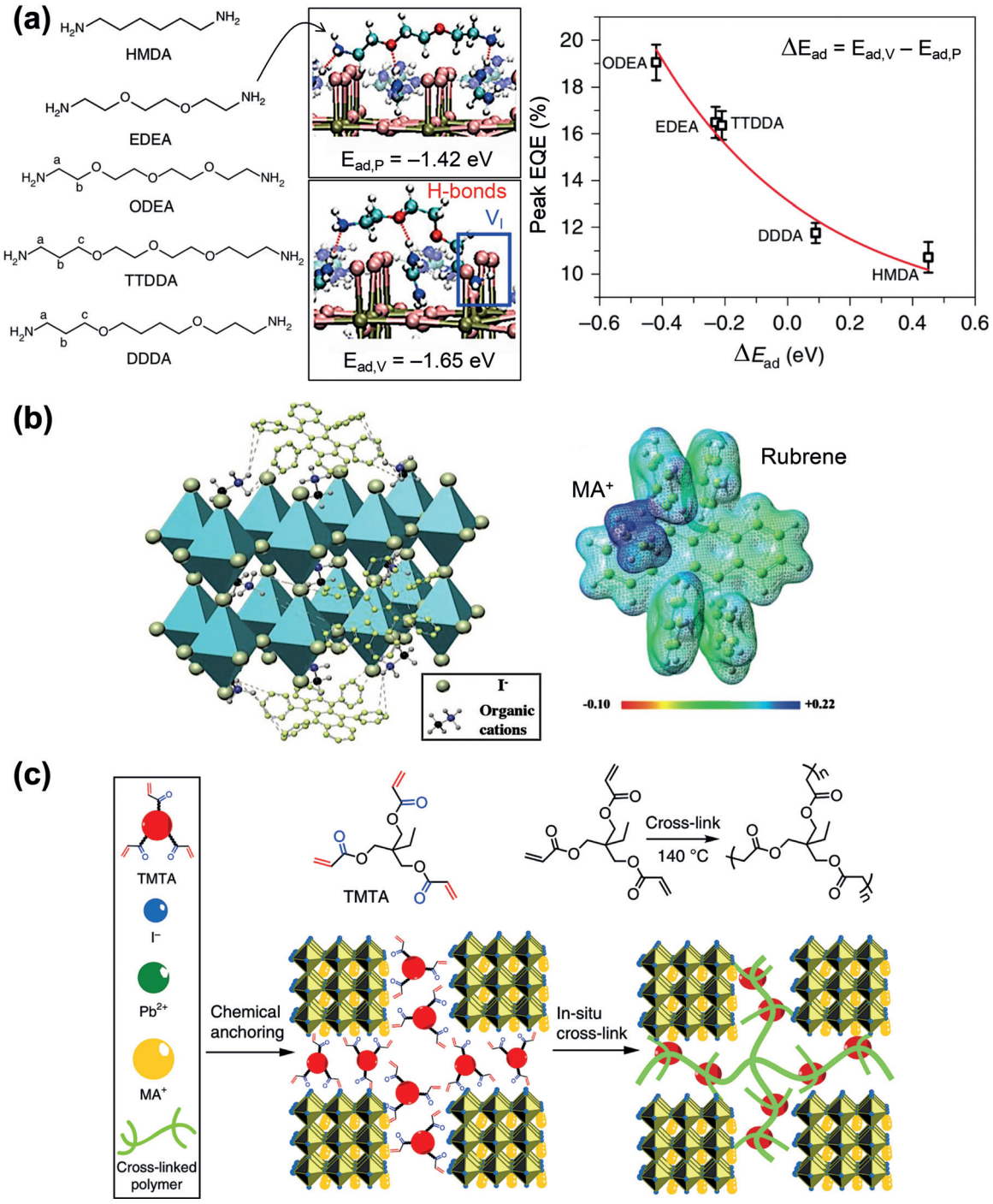

Figure 6. a) The molecular structures of HMDA, EDEA, ODEA, TTDDA, and DDDA for systematically varying the hydrogen bonds (H-bonds) strength and studying the interactions with FA^+ cations (dashed red lines) and iodide vacancy, V_I (blue box). Dependence of EQE values from various passivating molecules treated $FAPbI_3$-based perovskite LEDs. Reprinted with permission from Ref. [80]. Copyright 2019 Springer Nature Publishing AG. b) Mechanism of MA^+–π interaction between perovskite and rubrene molecule. DFT optimized configuration with electrostatic potential mesh maps. An interaction energy of −1.54 eV was computed. Reprinted with permission from Ref. [81]. Copyright 2018, WILEY-VCH Verlag GmbH & Co. KGaA, Weinheim. c) Illustration of cross-linked perovskite/polymer films. The chemical structure of TMTA monomer with marked carbonyl (blue) and alkenyl (red) groups. Cross-linking polymerization takes place upon annealing forming a continuous network of cross-linked polymer. Reprinted with permission from Ref. [82]. Copyright 2018 Springer Nature Publishing AG.

agreement with the previous discussion that the Lewis base strength of the passivating molecules plays a role in the coordination with under-coordinated Pb^{2+} defects; a soft Lewis base molecules is preferred in passivating under-coordinated Pb^{2+} defects.[63d] Further analyses suggest that the signal of $\Delta E_{ad} = E_{ad,V} - E_{ad,P}$ provides the preferential coordination with surface sites: the negative ΔE_{ad} indicates preferred interaction with V_I defects, while the positive ΔE_{ad}

indicates preferred interaction with FA^+ cations on defect-free surfaces (Figure 6a). In line with the rationale that hydrogen bonding can be weakened by introducing additional O atoms in the alkyl chain (accomplished by employing 2,2′-[oxybis(ethylenoxy)]diethylamine (ODEA)), and increased by elongating the length of the alkyl chain between N and O atoms (accomplished by employing 4,9-dioxa-1,12-dodecanediamine (DDDA) and 4,7,10-trioxa-1,13-tridecanediamine (TTDDA) molecules), the ΔE_{ad} concept was tested to quantify the external quantum efficiency (EQE) in perovskite LEDs (Figure 6a).

Similar to HMDA, DDDA is not an effective passivating molecule because its N and O atoms are almost isolated resulting in strong hydrogen bonding ability of amino groups. On the contrary, ODEA showed even a better passivation efficiency (EQE ≈ 19%) compared with EDEA because of its optimal hydrogen-bonding strength when interacting with under-coordinated Pb^{2+} defects (Figure 6a).[63d,91] These studies highlight a central message that not only the passivating functional groups are important, but also the molecular structure itself is key for the passivation effect and efficacy. Understanding of the fundamental physico-chemical properties of molecular structure is important for the design of more efficient passivation materials in the future.

Experimental evidence for desorption of MA^+ cations during thermal annealing and/or solar-cell operation leading to MA vacancies was also provided (Figure 5).[25b,50b,69a,92] Notably, the reports regarding cation (e.g., MA^+, FA^+, Cs^+) vacancy passivation is scarce.[63d,66,93] Although the MA vacancy is said to lead to only shallow trap states based on theoretical calculations (Figure 3a,b), its formation energy is low.[18b,28] Therefore, a high density of defects are still expected for the formation of MA^+ vacancies that leads to lowering in PCE as well as hysteresis phenomena.[50b,92b] The dipolar nature of MA^+ cations in mixed cation–halide perovskites were shown to play an important role in effectively healing deep trap defects leading to reduced trap-assisted non-radiative recombination processes.[50a,94] As a countermeasure, a few strategies have been reported to immobilize the A^+ cations.[62b,63j,81,95] For example, Wei et al.[81] showed that rubrene can interact strongly with MA^+ cations providing a calculated interaction energy of around 1.5 eV, which is sufficient to immobilize the organic cations and enhance perovskite surface stability (Figure 6b). The MA^+–rubrene interaction is electrostatic with an attractive force acting between the face of an electron-rich π system (aromatic π moieties) and adjacent MA^+ cation. This means that MA^+ cations covered with positive charge draw the neighboring polarizable π electrons from rubrene resulting in electron sharing at the junction of MA^+–rubrene (chelation-like cation–π interaction). Polymers were also widely applied in perovskites to reduce defect density and enhance thermal- and photo-stability (Table S2). In particular, studies employing polymer cross-linking (or cross-linking of functional monomers) started to gain attention because this strategy showed the ability to immobilize surface atoms/ions at grain boundaries and enhance material stability.[82,96] In the work by Li et al.,[82] the cross-linkable monomer of trimethylolpropane triacrylate (TMTA) was mixed into the $MAPbI_3$ perovskite precursor solution (Figure 6c). Three unique advantages of TMTA were proposed: 1) during perovskite crystallization TMTA is expelled to grain boundaries without interruption of the perovskite crystal growth; 2) the carbonyl groups in TMTA interact with PbI_2 leading to chemical anchoring to grain boundaries and further passivating defects; 3) the three alkenyl groups in TMTA allow cross-linking polymerization upon annealing (Figure 6c). TMTA-containing $MAPbI_3$-based PSCs showed an outstanding long-term stability and retained 80% of their initial efficiency after continuous power output at maximum power point (MPP) tracking for 400 h.[82] While the new research efforts utilizing multicomponent or chemical composition engineering have led to several best certified efficiencies in the NREL chart as well as enhanced stability, some researchers are developing strategies to simplify the perovskite composition to the basic ABX_3 formula (i.e., $MAPbI_3$, α,δ-$FAPbI_3$, $CsPbI_3$).[97] At the current stage, perovskite solar-cell stability is still far from reaching the >25 years lifetime,[97b] but recent studies have shown that ABX_3 perovskites can in fact present enhanced stability and can be more attractive to industry due to their simplicity in synthesis.[97,98]

In addition to charged defects, previous XPS studies have shown the existence of neutral species, such as unsaturated Pb^0 formed on the surface of perovskite induced by the oxidation of I^- into I_2 (Figure 1b).[5,99] Pb^0 is associated with a type of defect leading to deep trap state in perovskites.[100] Similarly, I^0 can also serve as carrier recombination centers.[101] Pb^0 and I^0 were identified to be generated during long-term operational stability under light, electric field, and thermal stress.[4,5,34b,99] More recently, Yang et al.[62b] have systematically studied the structures of passivation molecular functional groups, including carboxyl, amine, isopropyl, phenethyl, and *tert*-butylphenethyl groups to understand their passivation capabilities on the $Cs_{0.05}FA_{0.81}MA_{0.14}PbI_{2.55}Br_{0.45}$ perovskite. It was shown that carboxyl and amine groups heal charged defects via electrostatic interactions, and the number of neutral iodine (i.e., I_2) related defects can be reduced by the aromatic structures. The fundamental understanding of the underlying passivation mechanism allowed the researchers to design a new passivation molecule, D-4-*tert*-butylphenylalanine (D4TBP). Their solar-cell structure consisting of poly[bis(4-phenyl)(2,4,6-trimethylphenyl)amine] (PTAA)/ $Cs_{0.05}FA_{0.81}MA_{0.14}PbI_{2.55}Br_{0.45}$/ D4TBP/ fullerene (C60)/ 2,9-dimethyl-4,7-diphenyl-1,10-phenanthroline (BCP)/ copper (Cu) achieved a stabilized PCE of 21.4% with a V_{oc} of 1.23 V. As comparison, the pristine champion device generated a V_{oc} of 1.08 V and a PCE of 19.1%. Because the $Cs_{0.05}FA_{0.81}MA_{0.14}PbI_{2.55}Br_{0.45}$ perovskite has an optical band gap of 1.57 eV, this corresponds to a record low V_{oc} loss of 0.34 V in their devices after the D4TBP passivation. Alternatively, Wang et al.[34a] introduced a strategy for the constant elimination of Pb^0 and I^0 based on the incorporation of $Eu^{3+}\leftrightarrow Eu^{2+}$ as the "redox shuttle" that selectively oxidizes Pb^0 and reduces I^0 defects in a cyclical transition.[34b]

The interface engineering and defect passivation strategies led to the two points at 22.67%[102] and 23.32%[14] in the NREL certified efficiencies chart.[1a] In a recent work by Jung

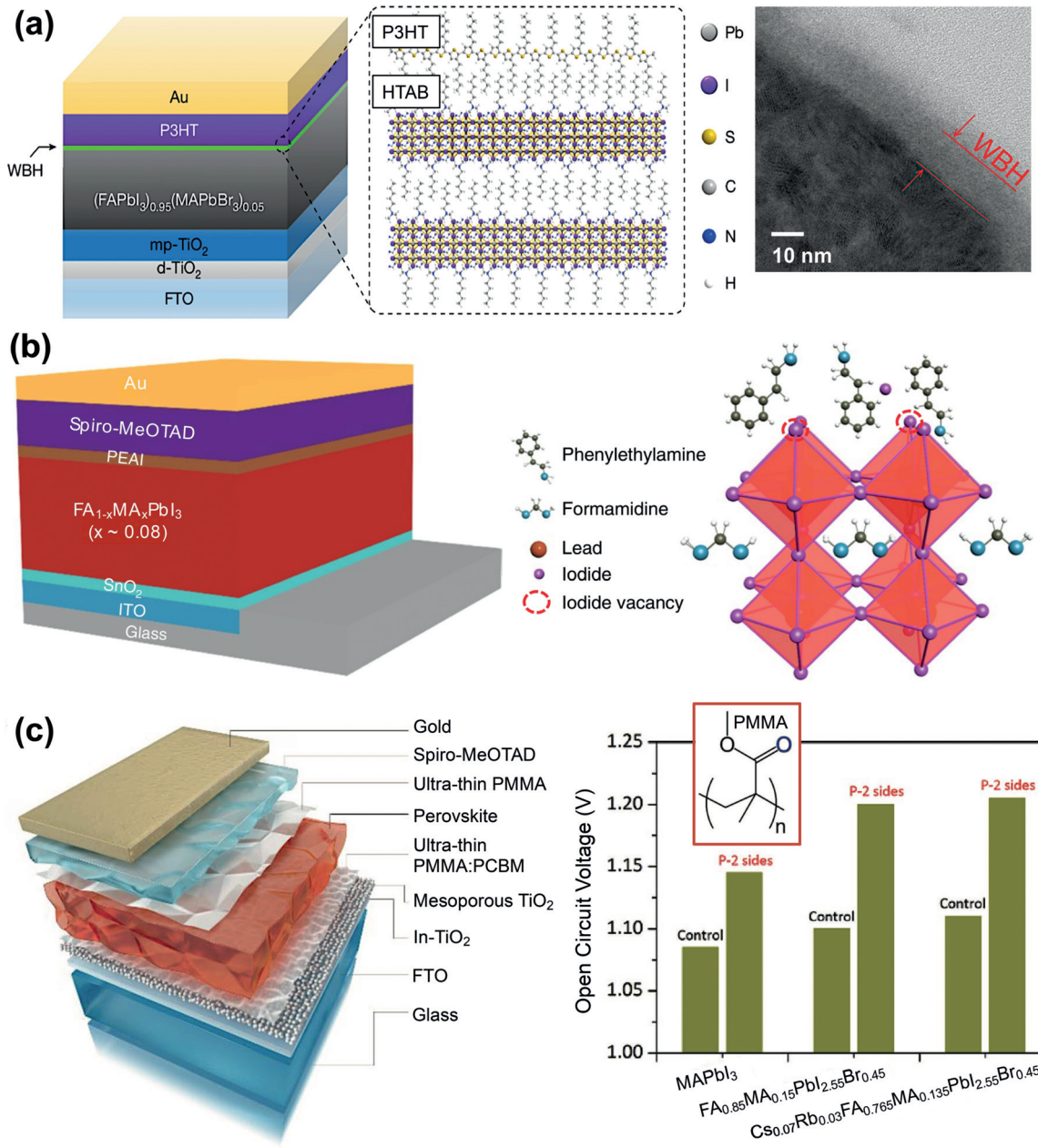

Figure 7. a) left: The perovskite solar-cell structure based on the wide band gap halide (WBH) structure by treating *n*-hexyl trimethyl ammonium bromide (HTAB) with $(FAPbI_3)_{0.95}(MAPbBr_3)_{0.05}$. The $(N^+(CH_3)_3^-)$ moiety in HTAB coordinates with defects in perovskites, while the aliphatic $(C_6H_{13}^-)$ moiety coordinates with P3HT via van der Waals interaction promoting self-assembled interdigitated structure between P3HT and HTAB (dashed box). Right: Cross-sectional high-resolution TEM image of WBH structure near the perovskite surface. Reprinted with permission from Ref. [102a]. Copyright 2019 Springer Nature Publishing AG. b) The perovskite solar-cell structure employing phenethylammonium iodide (PEAI) between $FA_{1-x}MA_xPbI_3$ ($x \approx 0.8$) perovskite and spiro-MeOTAD HTL. Proposed passivation mechanism: PEAI heals iodide vacancies exposing the underneath Pb^{2+} sites at the surfaces and grain boundaries. Reprinted with permission from Ref. [14]. Copyright 2019 Springer Nature Publishing AG. c) The perovskite solar cell structure with the strategy of double-sided passivated cells by an ultra-thin poly(methyl methacrylate) (PMMA) layer. V_{oc} distribution of perovskite solar cells comparing with the passivation (P-2 sides) and without the passivation (control). To confirm the universality of the double-side passivation approach, perovskites with different compositions were tested. Reprinted with permission from Ref. [103]. Copyright 2018, WILEY-VCH Verlag GmbH & Co. KGaA, Weinheim.

et al.,[102] *n*-hexyl trimethyl ammonium bromide (HTAB) was inserted between poly(3-hexylthiophene-2,5-diyl) regioregular (P3HT) and the perovskite layer, which resulted in the formation of a wide band gap halide (WBH) structure of $HTAB_{0.3}(FAPbI_3)_{0.95}(MAPbBr_3)_{0.05}$ (Figure 7a). The $(N^+(CH_3)_3^-)$ moiety in HTAB coordinates with defects in perovskites, while the aliphatic $(C_6H_{13}^-)$ moiety coordinates with P3HT via van der Waals interaction promoting self-assembly of P3HT on HTAB (Figure 7a). This interdigitation between alkyl chains of P3HT and HTAB leads to good hole-extraction and transport properties. Furthermore, the WBH structure led to the high certified PCE of 22.67% owing to

reduction of non-radiative recombination (defect passivation) and enhanced physical contact between perovskite and P3HT. In addition, this new HTL has the advantage over the commonly employed PTAA or spiro-MeOTAD HTLs because hygroscopic dopants are not required for enhancing hole mobility, which is beneficial for enhancing operational stability.[102] In another work, Jiang et al.[14] employed an organic halide salt of phenyl ethylammonium iodide (PEAI) as a passivation material (Figure 7b). PEAI was applied to the $FA_{1-x}MA_xPbI_3$ ($x \approx 0.08$) perovskite films by spin-coating, which helped suppress non-radiative recombination. This strategy led to the certified PCE of 23.32% in the NREL chart.[1a] PEAI coating on the perovskite layer was proposed to heal the defects by filling the iodide vacancies on the surface and at the grain boundaries.[14] A few studies[103,104] highlight the importance of double-side passivation in ensuring interface engineering of both sides of ETL/perovskite and perovskite/HTL (Figure 7c). This concept is similar to the device structure of passivated emitter and rear cell (PERC) in Si PV cells that rely on SiO_2 passivation at both front- and rear-side of a Si wafer.[104a,105] In the work by Peng et al.,[103] an ultra-thin insulating layer of poly(methyl methacrylate) (PMMA) was used as a double-side passivating polymer (Figure 7c). In addition to microstructure and surface morphology improvements,[106] the Lewis base nature of oxygen atoms in the carbonyl (C=O) groups in PMMA was ascribed as electron donors to reduce the charge state of Pb^{2+}, excess MA^+, and FA^+ charged defects. Double-sided PMMA passivated devices (P-2 sides; Figure 7c) demonstrated much higher V_{oc} than the corresponding non-passivated devices (control).[103] The studies above suggest that to further increase PCE of PSCs, strategies to improve V_{oc} and fill factor (FF) are needed, which can be achieved by defect passivation, because J_{sc} values have almost reached its limits (see the discussion on carrier management versus light management).[2,6b,14,104a,107]

As several reports have pointed out, charge neutrality is important when considering the passivation of charged defects in perovskites.[62a,b,66] Although several experimental studies discuss the formation and passivation of individual type of defects, formation of pair of defects (Schottky or Frenkel pair defects) are expected.[48a] Furthermore, while DFT results have shown that Frenkel defects (e.g., Pb^{2+}, I^-, Br^-, MA^+) lead to both deep and shallow trap states in perovskites,[23a,28] Schottky pair defects (e.g., PbI_2 and $PbBr_2$ vacancies and MAI and MABr vacancies) do not generate trap states within the band gap.[11c,108] The number of publications on the topic of passivation is increasing at a fast pace indicating that the perovskite community is aware of the paramount importance of passivation strategies to achieve reproducible high efficiency perovskite solar cells with long-term stability.[14,96,104a,109]

4. Summary and Outlook

As the fundamental origin, structural defects, and impurities in semiconductor materials play an important role in the overall performance of electronic devices in general.[8,91,110] In several photovoltaic technologies (e.g., Si, CIGS, CdTe), the presence of electronic defects within the semiconductor band gap limits the efficiency, reproducibility, as well as stability/lifetime.[7a] Therefore, efforts have been made in the direction to minimize the defect density by well-controlled semiconductor fabrication technology. The reported conventional semiconductors has defect densities of 10^{14} cm^{-3} (polycrystalline Si), 10^{13} cm^{-3} (CIGS), 10^{15} cm^{-3} (CdTe).[23f] Unlike crystalline Si solar cells, which are fabricated via a well-controlled semiconductor manufacturing technology, perovskite solar cells are fabricated via a solution-based methods (e.g., spin-coating, blade-coating, spray-coating)[102a,111] and vapor-based techniques[112] where the crystal-growth kinetics are generally fast.[24a] In addition, often the annealing as post-treatment is required with the aim to remove the remaining solvent, which often leads to a wide range of defects.[11c,23c,24b,25,113] These imperfect lattice alignments can be of a short range due to point defects or impurity atoms/ions (Figure 2b–d,f or of a long range due to 1D dislocations, 2D grain boundaries, and 3D precipitates (Figure 2b,e,g). As a consequence, these structural defects will induce the generation of electron and hole carriers traps within the band gap. The trap states can potentially act as scattering centers and non-radiative recombination centers leading to deterioration in photophysical properties. Therefore, a thorough characterization of these defects, such as 1) experimentally assigned type of defects present in perovskites, 2) defects densities, and 3) the energy positions of these defects within the band gap is important. In earlier studies, efforts have been made to slow down the perovskite crystallization kinetics and improve crystallinity (i.e., larger grain sizes) by adding dimethyl sulfoxide (DMSO), *N*-methyl-2-pyrrolidone (NMP), and 1,8-diiodooctane (DIO)[114] additives into the perovskite precursor solutions to form complexes with PbI_2.[66,68a] However, even slight variations in the parameters of these solution-based methods are still expected to lead to large variations in the concentration of defect densities during fabrication processes. Although it is still possible to attain high efficiencies on lab scale solar cells with an active area less than 1 cm^2, the uncontrolled high/low density of defects are expected to be one of the main factors that influence the efficiency variations from batch-to-batch (i.e., non-reproducibility) as well as leading to challenges in upscaling.[115] Furthermore, a relationship between the quality of perovskite polycrystalline films and the stability of devices was described.[116] Often the perovskite polycrystalline films have an undefined chemical composition at the grain boundaries and may lead to a new set of structural defects.[23d,117] It has been shown that moisture-sensitive defects at grain boundaries play an important role in triggering the moisture-induced degradation process.[116b] The situation is more complex when considering the influences of interfaces formed between perovskite and its adjacent layer (e.g., at the interface between TiO_2 and perovskite).[102b,118] Therefore, characterization and control of defect formation and its concentration are of paramount importance for achieving reproducible high efficiency perovskite solar cells with large area and long-term stability.[6b,98b,119]

Efforts have been made to theoretically identify the different types of point defects in perovskites.[23d,117] However, it is important to note that the identification of the different types of defects experimentally is imperative but challenging. In this sense, the defect passivation strategies employed in perovskites provide indications for deducing the type of defects existing in perovskites by analyzing the coordination chemistry between the passivating molecule and perovskite surface. Combining the passivation strategies and analytical tools (TAS, DLTS, SSPL, TRMC, TSC, C-f, TPC, temperature dependent *I–V* measurements and summarized in Table S1) are observed to provide the thorough pictures of the type of defects and quantify the energy levels that lead to trap states and their respective density. Regarding passivation strategies, two methodologies are commonly employed (Table S2). The choices of passivation molecules by rational design are either: 1) added in the perovskite precursor solution (29 out of the 72 studies surveyed in this Review),[120] or 2) employed in the post-treatment step (43 out of the 72 studies surveyed in this Review).[76,121] Both methods have been shown to be effective in enhancing the device stability and performance. Our survey shown in Table S2 and summarized in Figure 1b provides a comprehensive list of the types of defects deduced by the passivation strategy employing FTIR, XPS, TOF-SIMS, Raman, and EDX spectroscopy.

A large number of publications report: 1) halide vacancies (e.g., Cl^-, Br^-, I^-) leading to exposure of under-coordinated positively charged Pb^{2+} atoms (29 out of the 72 studies surveyed in this Review). The subsequent larger number of publications deals on 2) negatively charged Pb–I anti-sites (PbI_3^-) or halide-excess (16 out of 72), followed by 3) cation vacancies surface termination (e.g., Cs^+, MA^+; 6 out of the 72 studies surveyed in this Review), 4) mobile or volatile iodine and MA^+ cation (4 out of the 72 studies surveyed in this Review), 5) metallic lead (Pb^0) surface terminated (3 out of the 72 studies surveyed in this Review), and 6) I^0 (I_2) defects (2 out of the 72 studies surveyed in this Review). Because multiple different types of defects are present, it is important to adopt passivating molecules that have dual functions of Lewis base and Lewis acid to passivate effectively both types of positively and negatively charged defects simultaneously (Figure 5).[56b,62,66,69a,89a–e] However, for instance, even though a perovskite surface "free" of charged defects is attained, there is evidence that halides located at the grain boundaries are mobile under an electric field. In addition, desorption of MA^+ cations is known to occur even during mild thermal annealing and/or solar cell operation conditions.[4,5,27a–d,69a,98b,122] In our view, the development of designing molecules that can anchor the under-coordinated halides and under-coordinated cations without disrupting charge excitation and transport in perovskites deserves further attention, but currently the number of reports on this topic is still scarce.[65,69b,89d] Strategies of making stronger interactions between A^+ cations (MA^+, FA^+, Cs^+) and $[PbX_6]^{4-}$ (X = I, Br) octahedra helps stabilize the perovskite.[76] Acquiring a complete fundamental understanding of defects in perovskites is highly desirable not only for improving solar-cell efficiencies, but for enhancing other technologically relevant issues for commercialization (efficiency of solar modules, upscaling, reproducibility, and stability). For example, defects such as halide vacancies and under-coordinated Pb^{2+}, were associated as being moisture-sensitive and react easily with H_2O and O_2 and therefore a rational design of polymers with one end that attaches to defects in perovskites and the other end with a hydrophobic functionalization was shown to be effective.[49b,76,123]

On the basis of our survey (Table S2), another key message is that none of the passivation strategies can eliminate the defects completely and they can only reduce the defect density to a certain degree (1 to 2 orders of magnitude lower).[54f–i,56a,b,62a,b,66,72,73,76,89e,124] In all of these studies, the TAS technique was the main technique employed to compare the defect densities before and after the passivation. As described above, these defects in perovskites lead to trap-assisted recombination processes and naturally a question arises as to what is the maximum threshold of defect concentration tolerable for influencing minimally on solar cell performance. The detailed balance model provides insights into this question.[125] Provided that the defect density is significantly lower than the density of free carriers generated under solar-cell operation conditions, the impact of defect density on the charge-carrier transport will be minimal.[68a] Experimentally, defect densities of 5.8×10^9 cm^{-3} and 3.3×10^{10} cm^{-3} were reported for $MAPbBr_3$ and $MAPbI_3$ single crystals, respectively.[43b,d,54e] In comparison, polycrystalline $MAPbI_3$ thin films have shown a larger density of defects in the order of 10^{15} cm^{-3} to 10^{17} cm^{-3} (Figure 1).[90e] Stoumpos et al.[17a] reported intrinsic carrier densities for $MAPbI_3$ crystals from both thermopower ($<10^{16}$ cm^{-3}) and Hall effect measurements (ca. 10^9 cm^{-3}).[125c] The Hall effect measurements reported by Wang et al.[122] showed that the intrinsic carrier concentration varies with the perovskite stoichiometry. $MAPbI_3$ polycrystalline films formed from stoichiometric precursor solution (PbI_2/MAI = 1:1 molar ratio) lead to heavily n-doped semiconductors with an electron concentration of 2.8×10^{17} cm^{-3}. Reducing the precursor ratio to 0.3:1 (PbI_2 : MAI) converted the films into weak p-type semiconductors with a low hole concentration on the order of 10^{14} cm^{-3}.[126] On the basis of these numbers, it is likely that a defect density on the order of 10^{14} cm^{-3} or lower in the polycrystalline thin films is the upper bound threshold for achieving high performances in solar cells and especially solar modules.[127] Grain boundaries and interfaces are prone to defect formation. Therefore, it is often preferable to form perovskite films with larger grains. The surface area to volume ratio is an important parameter, which was reported to influence the defect formation energy (DFE) by Meggiolaro et al. (in Figure 8a,b).[90c,128] We define the initial solar cell PCE to be PCE($t=0$). The PCE varies as a function of its operation time before the cell completely decays, $0 < \mathrm{PCE}(t) < \mathrm{PCE}(t=0)$. This PCE evolution is strongly correlated with the defect generation, defect migration, halide segregation, volatilization of cations and anions, metallic-Pb formation.[129] In addition, these dynamic physico-chemical processes are dominated by surfaces and grain boundaries, that is, perovskite polycrystalline films with smaller grain sizes tend to show a lower PCE and shorter lifetime.[116b] Therefore, if we can estimate the defect density corresponding to the upper

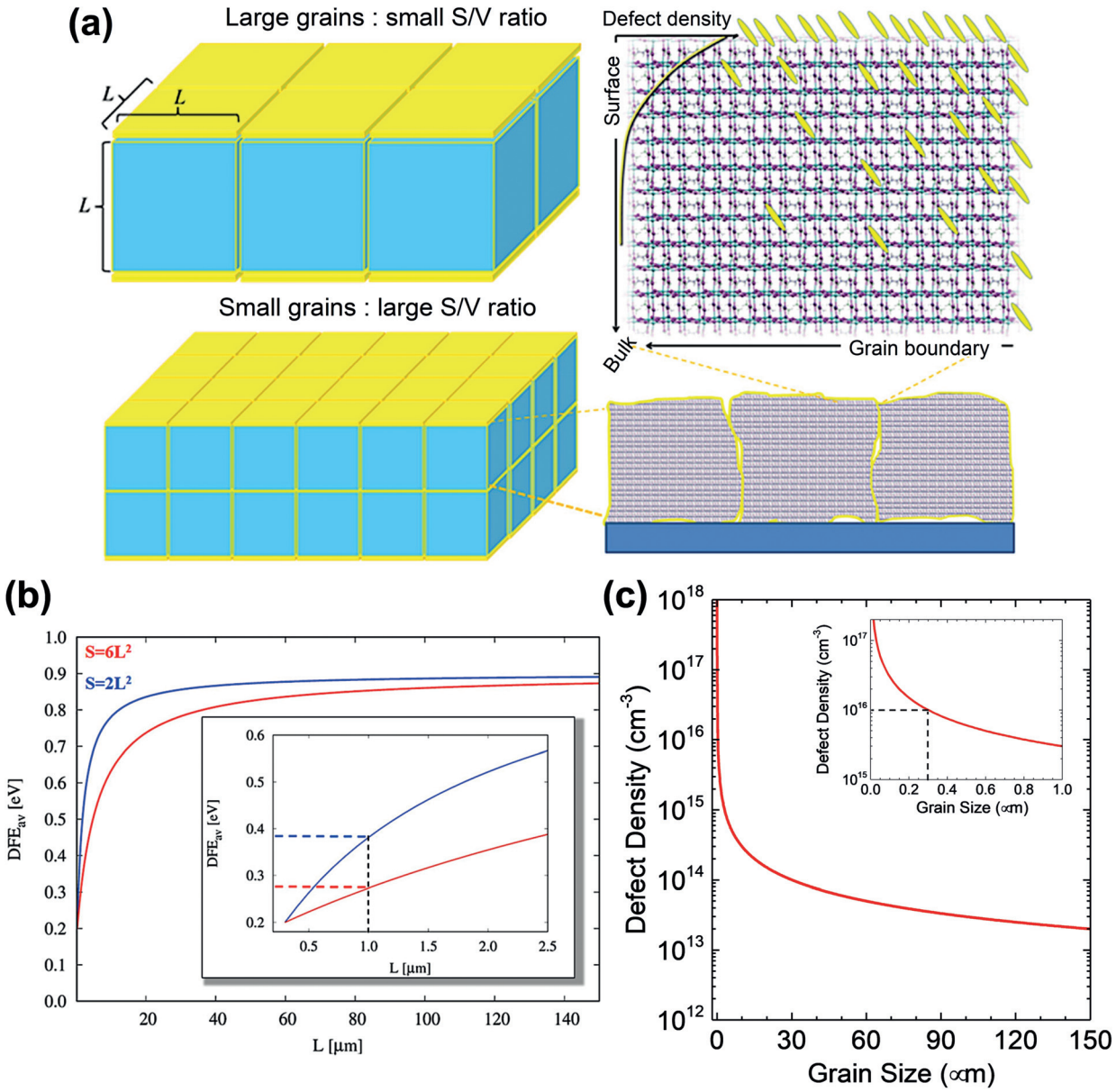

Figure 8. a) Schematic illustration showing the difference of the surface/volume ratio for perovskite films with large and small grains (L = the length of each side if assuming a cubic grain). The drastic increase in the defect density distribution varying from the bulk to surface (or grain boundary) is highlighted. b) Average defect formation energy (DFE_{av}) as a function of crystal grain size for 2 different surface estimates ($6L^2$ and $2L^2$). Reprinted with permission from Ref. [90c]. Copyright 2019 American Chemical Society. c) Estimated upper limit of the surface defect density as a function of crystal grain size for a reasonable working perovskite solar cell. Grain sizes of around 300 nm show a defect density of approximately 10^{16} cm^{-3}, which is in good agreement with experimental results (10^{16} to 10^{17} cm^{-3}; Figure 1a and Table S1).

bound value and compare this value to experimentally extracted defect density, we can determine whether a perovskite film in a solar cell has a reasonably high polycrystalline film quality. We estimate the density of defects as a function of grain size considering geometrical parameters. For simplicity, we assume a cubic-shaped $MAPbI_3$ grain with L as the grain size dimension, where the total available surface sites (including grain boundaries) scales as approximately $6L^2$, while the volume scales as approximately L^3 (Figure 8a).[90c] We consider, for instance, the generation of at least two detrimental defects (meaning the generation of a Frenkel or a Schottky pair defect that considers the overall charge neutrality) per surface unit cell for $MAPbI_3$ (lattice constant of ca. 6.3 Å),[24b,48c] which leads to a surface defect density of $d_{surface} \approx 5 \times 10^{14}$ cm^{-2}. The density of defects as a function of grain size can be expressed by approximately $(d_{surface} \times 6L^2 + d_{bulk} \times L^3)/L^3$, where d_{bulk} is the volumetric density of bulk defect sites.[90c] Several studies have proposed that for perovskite solar cells, relevant defects are predominantly located at surfaces, interfaces and/or grain boundaries, and the number of defects in bulk is significantly fewer. With the assumption that the defect density in the bulk is negligible compared to the surface defect density, for L = 300 nm (see the inset in Figure 8c), a surface defect density of approx-

imately 10^{16} cm^{-3}, can be derived, which is roughly the same as the experimentally measured defect density in perovskite films with a typical defect density in the range from 10^{15} to 10^{17} cm^{-3} (Figure 1a and Table S1). This agreement in turn verifies that it is most likely correct to assume that in solar cells based on perovskite films, surface defects are the most important ones. In addition, on the basis of experimental results on the total defect density in perovskite solar cells (Table S1), $d_{bulk} \approx 10^{10}$ cm^{-3} can be inferred when considering large crystal grain size ($L \rightarrow \infty$).[54g,90c] Using this estimation, perovskite solar cells based on thin-sliced "perfect" single crystals or single-crystalline-membranes can be promising for attaining both enhanced efficiency and stability.[54a,f–i,55a,130] A recent study employing single-crystal $CH_3NH_3PbI_3$ perovskite sample (thickness = 20 μm) showed an outstanding PCE of 21.09% and FF up to 84.3%.[90a]

Despite the superior properties of Pb-based perovskites, the toxicity of Pb is a concern to investors and consumers, because possible Pb leakage during fabrication, installation, or disposal can severely contaminate environment and harm human beings.[119f,131] It will be desirable to obtain an in-depth understanding about the mechanisms at the origin of the defect-tolerant property and find alternative semiconductor materials with such properties. On the basis of theoretical calculations,[23d,29,117,132] the electronic structure nature of bonding and antibonding character was proposed as a possible origin for the defect tolerance in Pb-based perovskites. In several semiconductors, the VB edge is composed of bonding states, while the CB edge is composed of antibonding states. These materials (e.g., GaAs, GaN, Si, CdSe) are often sensitive to structural defects (i.e., defect intolerant; Figure 3c) because the removal of constituent elements leads to the appearance of defect states within CB (antibonding) and VB (bonding) edges (Figure 3c). On the other hand, some semiconductors (e.g., CIGS, Cu_3N, CdTe) with the electronic structure of the VB edge composed of antibonding character and the CB edge composed of bonding character demonstrate defect tolerance. In such semiconductors, the defect states that result from removal or insertion of constituent elements into the crystal structure fall within the VB or CB bands instead of inside the band gap (Figure 3c). In $MAPbI_3$, a similar defect-tolerance argument can be applicable for valence band derived defect states such as V_{Pb} and V_{MA} (Figure 3a,c). In the case of V_I that also shows a low formation energy (Figure 3a,b), the resulting dangling bonds appear as defect states inside CB. In addition, 1) relativistic effects push the CB edge energy down;[132d] 2) the interaction between Pb 6s^2 lone-pair electrons and I 5p orbitals results in strong coupling to push the VB edge energy higher (both (1) and (2) help the defect-state energies reside outside the band gap);[117,132b] 3) the CB edge has ionic character (i.e., CB is derived from the Pb^{2+} p orbital with a minimum contribution from other constituent elements; hence, the ionic nature of the CB edge indicates that structural defects may not alter the energy level of CB);[23d,117] 4) small capture cross sections of charged defects because of screening by a high dielectric constant[29,132d] and 5) self-healing[133] were additionally proposed as contributing factors for defect tolerance in perovskites. Xiao et al.[132c] analyzed the several Pb-based and Pb-free halide perovskites that have the structures of 3D, 2D layers, 1D chains, and 0D isolated octahedra. Crystalline structural dimensionality has been often used as a figure of merit to evaluate photovoltaic properties (e.g., 3D structures often lead to smaller band gaps; charge transport in isotropic 3D structured perovskites is much smoother compared to that in randomly oriented grains, such as 2D, 1D, and 0D). This concept is demonstrated to be valid for some absorbers, but it fails for some others. For example, double perovskites such as $Cs_2AgBiBr_6$ have the 3D structure, but the reported PCEs are much lower. To address this deficiency (i.e., the structural dimensionality concept fails in some cases), they introduced the new concept of electronic dimensionality, which describes the connectivity or the overlapping of the atomic orbitals forming the conduction and valence band edges.[132c] Higher electronic dimensionality (e.g., $MAPbI_3$) is associated with both conduction- and valence-band edge derived orbitals connecting three-dimensionally. Because of this 3D electronic dimensionality, both conduction and valence band edges have band dispersion extending in all directions, leading to isotropic (3D) charge transport properties with fewer recombination events.[132c] In comparison, perovskites with lower electronic dimensionality (e.g., $Cs_2AgBiBr_6$ double perovskite) are associated with 1) conduction or valence band edge derived orbitals that cannot connect three-dimensionally; 2) mismatch in angular momentum of conduction or valence band edge derived orbitals leading to indirect band gaps; 3) large carrier effective masses along some directions in 0D electronic dimensional perovskites; and 4) the presence of dominant defects (with low formation energies) leading to deep-level electronic trap states. On the basis of these analyses,[132c] $Cs_2AgBiBr_6$ double perovskite does not exhibit promising photovoltaic properties comparable to $MAPbI_3$. This report emphasizes that not only light management (i.e., the band gap dependent J_{sc}/J_{SQ} where SQ is the Shockley-Queisser limit) but also charge carrier management ($(V_{oc} \times FF)/(V_{SQ} \times FF_{SQ})$ or the electronic transport) causes the generally lower PCEs reported in lower-dimensional (2D, 1D, and 0D) perovskites.[2,6b,14,104a,107] Further research efforts are underway to understand better defect tolerance and its origin in perovskites, which may help predict other novel materials with defect tolerance properties as well as enhanced stability and minimal toxicity. Experimental advancements in material science for the synthesis of new semiconducting materials are moving at a fast pace. However, it is imperative to reach 1) a comprehensive microscopic picture of the types of defects considering various constraints (e.g., the overall charge neutrality, the conservation of mass during degradation etc.), 2) its origin, for example, their generation in different stages during sample preparation and degradation under device operation (Figure 1c), and 3) remedies to minimize detrimental defects.

Acknowledgements

This work was supported by funding from the Energy Materials and Surface Sciences Unit of the Okinawa Institute

of Science and Technology Graduate University, the OIST R&D Cluster Research Program, the OIST Proof of Concept (POC) Program, and JSPS KAKENHI Grant Number JP18K05266. S.L. acknowledges the funding support from the 111 Project (B14041).

Conflict of interest

The authors declare no conflict of interest.

How to cite: *Angew. Chem. Int. Ed.* **2020**, *59*, –
Angew. Chem. **2020**, *132*, –

[1] a) National Renewable Energy Laboratory (NREL). Research Cell and Module Efficiency Records, https://www.nrel.gov/pv/cell-efficiency.html und https://www.nrel.gov/pv/module-efficiency.html, (Zugriff am 24. Juli 2019); b) M. A. Green, Y. Hishikawa, E. D. Dunlop, D. H. Levi, J. Hohl-Ebinger, M. Yoshita, A. W. Y. Ho-Baillie, *Prog. Photovolt. Res. Appl.* **2019**, *27*, 3 – 12.

[2] A. Polman, M. Knight, E. C. Garnett, B. Ehrler, W. C. Sinke, *Science* **2016**, *352*, aad4424.

[3] C. Battaglia, A. Cuevas, S. De Wolf, *Energy Environ. Sci.* **2016**, *9*, 1552 – 1576.

[4] S. Wang, Y. Jiang, E. J. Juarez-Perez, L. K. Ono, Y. B. Qi, *Nat. Energy* **2016**, *2*, 16195.

[5] E. J. Juarez-Perez, L. K. Ono, M. Maeda, Y. Jiang, Z. Hawash, Y. B. Qi, *J. Mater. Chem. A* **2018**, *6*, 9604 – 9612.

[6] a) Fraunhofer Institute for Solar Energy Systems ISE, https://www.ise.fraunhofer.de/en.html, (Zugriff am 14. Mai 2019); b) L. K. Ono, Y. B. Qi, *J. Phys. D* **2018**, *51*, 093001.

[7] a) J. S. Park, S. Kim, Z. Xie, A. Walsh, *Nat. Rev. Mater.* **2018**, *3*, 194 – 210; b) Y. Zhang, *Chin. Phys. B* **2018**, *27*, 117103.

[8] H. J. Queisser, E. E. Haller, *Science* **1998**, *281*, 945 – 950.

[9] L. D. Whalley, J. M. Frost, Y.-K. Jung, A. Walsh, *J. Chem. Phys.* **2017**, *146*, 220901.

[10] K. Yoshikawa, H. Kawasaki, W. Yoshida, T. Irie, K. Konishi, K. Nakano, T. Uto, D. Adachi, M. Kanematsu, H. Uzu, K. Yamamoto, *Nat. Energy* **2017**, *2*, 17032.

[11] a) Y. Yan, W.-J. Yin, Y. Wu, T. Shi, N. R. Paudel, C. Li, J. Poplawsky, Z. Wang, J. Moseley, H. Guthrey, H. Moutinho, S. J. Pennycook, M. M. Al-Jassim, *J. Appl. Phys.* **2015**, *117*, 112807; b) T. W. Kim, S. Uchida, T. Matsushita, L. Cojocaru, R. Jono, K. Kimura, D. Matsubara, M. Shirai, K. Ito, H. Matsumoto, T. Kondo, H. Segawa, *Adv. Mater.* **2018**, *30*, 1705230; c) C. Ran, J. Xu, W. Gao, C. Huang, S. Dou, *Chem. Soc. Rev.* **2018**, *47*, 4581 – 4610.

[12] F. Bussolotti, S. Kera, K. Kudo, A. Kahn, N. Ueno, *Phys. Rev. Lett.* **2013**, *110*, 267602.

[13] a) D. M. Jonathan, *Semicond. Sci. Technol.* **2016**, *31*, 093001; b) J. A. Carr, S. Chaudhary, *Energy Environ. Sci.* **2013**, *6*, 3414 – 3438; c) L. G. Kaake, P. F. Barbara, X. Y. Zhu, *J. Phys. Chem. Lett.* **2010**, *1*, 628 – 635.

[14] Q. Jiang, Y. Zhao, X. Zhang, X. Yang, Y. Chen, Z. Chu, Q. Ye, X. Li, Z. Yin, J. You, *Nat. Photonics* **2019**, *13*, 460 – 466.

[15] a) A. Kojima, K. Teshima, Y. Shirai, T. Miyasaka, *J. Am. Chem. Soc.* **2009**, *131*, 6050 – 6051; b) T. Miyasaka, *Bull. Chem. Soc. Jpn.* **2018**, *91*, 1058 – 1068; c) A. K. Jena, A. Kulkarni, T. Miyasaka, *Chem. Rev.* **2019**, *119*, 3036 – 3103.

[16] a) H. S. Kim, C. R. Lee, J. H. Im, K. B. Lee, T. Moehl, A. Marchioro, S. J. Moon, R. Humphry-Baker, J. H. Yum, J. E. Moser, M. Grätzel, N. G. Park, *Sci. Rep.* **2012**, *2*, 591; b) N.-G. Park, *MRS Bull.* **2018**, *43*, 527 – 533.

[17] a) C. C. Stoumpos, C. D. Malliakas, M. G. Kanatzidis, *Inorg. Chem.* **2013**, *52*, 9019 – 9038; b) C. C. Stoumpos, M. G. Kanatzidis, *Adv. Mater.* **2016**, *28*, 5778 – 5793; c) B. Saparov, D. B. Mitzi, *Chem. Rev.* **2016**, *116*, 4558 – 4596; d) F. Zhu, L. Men, Y. Guo, Q. Zhu, U. Bhattacharjee, P. M. Goodwin, J. W. Petrich, E. A. Smith, J. Vela, *Acs Nano* **2015**, *9*, 2948 – 2959; e) T. Oku, in *Solar Cells-New Approaches and Reviews* (Ed.: L. A. Kosyachenko), InTech, Rijeka, **2015**, pp. 77 – 102.

[18] a) D. A. Egger, A. Bera, D. Cahen, G. Hodes, T. Kirchartz, L. Kronik, R. Lovrincic, A. M. Rappe, D. R. Reichman, O. Yaffe, *Adv. Mater.* **2018**, *30*, 1800691; b) Q. A. Akkerman, G. Rainò, M. V. Kovalenko, L. Manna, *Nat. Mater.* **2018**, *17*, 394 – 405; c) J.-W. Lee, S.-G. Kim, J.-M. Yang, Y. Yang, N.-G. Park, *APL Mater.* **2019**, *7*, 041111.

[19] R. Ohmann, L. K. Ono, H.-S. Kim, H. Lin, M. V. Lee, Y. Li, N.-G. Park, Y. B. Qi, *J. Am. Chem. Soc.* **2015**, *137*, 16049 – 16054.

[20] M. Yang, Y. Zhou, Y. Zeng, C.-S. Jiang, N. P. Padture, K. Zhu, *Adv. Mater.* **2015**, *27*, 6363 – 6370.

[21] Y. Zhou, M. Yang, A. L. Vasiliev, H. F. Garces, Y. Zhao, D. Wang, S. Pang, K. Zhu, N. P. Padture, *J. Mater. Chem. A* **2015**, *3*, 9249 – 9256.

[22] W. Tress, *Adv. Energy Mater.* **2017**, *7*, 1602358.

[23] a) W.-J. Yin, T. Shi, Y. Yan, *Appl. Phys. Lett.* **2014**, *104*, 063903; b) W. J. Yin, J. H. Yang, J. Kang, Y. F. Yan, S. H. Wei, *J. Mater. Chem. A* **2015**, *3*, 8926 – 8942; c) J. M. Ball, A. Petrozza, *Nat. Energy* **2016**, *1*, 16149; d) Z. Xiao, Y. Yan, *Adv. Energy Mater.* **2017**, *7*, 1701136; e) J. M. Azpiroz, E. Mosconi, J. Bisquert, F. De Angelis, *Energy Environ. Sci.* **2015**, *8*, 2118 – 2127; f) D. Meggiolaro, F. De Angelis, *ACS Energy Lett.* **2018**, *3*, 2206 – 2222; g) D. Meggiolaro, E. Mosconi, F. De Angelis, *ACS Energy Lett.* **2018**, *3*, 447 – 451.

[24] a) Y. Zhou, O. S. Game, S. Pang, N. P. Padture, *J. Phys. Chem. Lett.* **2015**, *6*, 4827 – 4839; b) L. K. Ono, Y. B. Qi, *J. Phys. Chem. Lett.* **2016**, *7*, 4764 – 4794; c) I. M. Hermes, S. A. Bretschneider, V. W. Bergmann, D. Li, A. Klasen, J. Mars, W. Tremel, F. Laquai, H.-J. Butt, M. Mezger, R. Berger, B. J. Rodriguez, S. A. L. Weber, *J. Phys. Chem. C* **2016**, *120*, 5724 – 5731; d) E. Strelcov, Q. Dong, T. Li, J. Chae, Y. Shao, Y. Deng, A. Gruverman, J. Huang, A. Centrone, *Sci. Adv.* **2017**, *3*, e1602165; e) H. Röhm, T. Leonhard, M. J. Hoffmann, A. Colsmann, *Energy Environ. Sci.* **2017**, *10*, 950 – 955; f) M. U. Rothmann, W. Li, Y. Zhu, U. Bach, L. Spiccia, J. Etheridge, Y.-B. Cheng, *Nat. Commun.* **2017**, *8*, 14547.

[25] a) J. Chen, N.-G. Park, *Adv. Mater.* **2018**, *30*, 1803019; b) Y. Yuan, J. Huang, *Acc. Chem. Res.* **2016**, *49*, 286 – 293; c) Y. Zhang, Y. Wang, Z. Q. Xu, J. Liu, J. Song, Y. Xue, Z. Wang, J. Zheng, L. Jiang, C. Zheng, F. Huang, B. Sun, Y. B. Cheng, Q. Bao, *Acs Nano* **2016**, *10*, 7031 – 7038; d) J. Hieulle, C. Stecker, R. Ohmann, L. K. Ono, Y. B. Qi, *Small Methods* **2018**, *2*, 1700295.

[26] W. Li, S. K. Yadavalli, D. Lizarazo-Ferro, M. Chen, Y. Zhou, N. P. Padture, R. Zia, *ACS Energy Lett.* **2018**, *3*, 2669 – 2670.

[27] a) M.-C. Jung, Y. M. Lee, H.-K. Lee, J. Park, S. R. Raga, L. K. Ono, S. Wang, M. R. Leyden, B. D. Yu, S. Hong, Y. B. Qi, *Appl. Phys. Lett.* **2016**, *108*, 073901; b) E. J. Juarez-Perez, Z. Hawash, S. R. Raga, L. K. Ono, Y. B. Qi, *Energy Environ. Sci.* **2016**, *9*, 3406 – 3410; c) E. J. Juarez-Perez, L. K. Ono, I. Uriarte, E. J. Cocinero, Y. B. Qi, *ACS Appl. Mater. Interfaces* **2019**, *11*, 12586 – 12593; d) A. García-Fernández, E. J. Juarez-Perez, S. Castro-García, M. Sánchez-Andújar, L. K. Ono, Y. Jiang, Y. B. Qi, *Small Methods* **2018**, *2*, 1800242; e) A. Latini, G. Gigli, A. Ciccioli, *Sustainable Energy Fuels* **2017**, *1*, 1351 – 1357; f) Z. Song, C. Wang, A. B. Phillips, C. R. Grice, D. Zhao, Y. Yu, C. Chen, C. Li, X. Yin, R. J. Ellingson, M. J. Heben, Y. Yan, *Sustainable Energy Fuels* **2018**, *2*, 2460 – 2467; g) A. Dualeh, P. Gao, S. I. Seok, M. K. Nazeeruddin, M. Grätzel, *Chem. Mater.* **2014**, *26*, 6160 – 6164; h) J. Chun-Ren Ke, A. S. Walton, D. J. Lewis, A. Tedstone, P. O'Brien, A. G. Thomas, W. R. Flavell, *Chem. Commun.* **2017**, *53*, 5231 – 5234; i) R.-P. Xu, Y.-Q. Li, T.-

Y. Jin, Y.-Q. Liu, Q.-Y. Bao, C. O'Carroll, J.-X. Tang, *ACS Appl. Mater. Interfaces* **2018**, *10*, 6737 – 6746.
[28] W.-J. Yin, T. Shi, Y. Yan, *Adv. Mater.* **2014**, *26*, 4653 – 4658.
[29] R. E. Brandt, J. R. Poindexter, P. Gorai, R. C. Kurchin, R. L. Z. Hoye, L. Nienhaus, M. W. B. Wilson, J. A. Polizzotti, R. Sereika, R. Žaltauskas, L. C. Lee, J. L. MacManus-Driscoll, M. Bawendi, V. Stevanović, T. Buonassisi, *Chem. Mater.* **2017**, *29*, 4667 – 4674.
[30] G. Landi, H. C. Neitzert, C. Barone, C. Mauro, F. Lang, S. Albrecht, B. Rech, S. Pagano, *Adv. Sci.* **2017**, *4*, 1700183.
[31] Y. Shao, Y. Yuan, J. Huang, *Nat. Energy* **2016**, *1*, 15001.
[32] a) S. R. Raga, M.-C. Jung, M. V. Lee, M. R. Leyden, Y. Kato, Y. B. Qi, *Chem. Mater.* **2015**, *27*, 1597 – 1603; b) B. Conings, J. Drijkoningen, N. Gauquelin, A. Babayigit, J. D'Haen, L. D'Olieslaeger, A. Ethirajan, J. Verbeeck, J. Manca, E. Mosconi, F. D. Angelis, H.-G. Boyen, *Adv. Energy Mater.* **2015**, *5*, 1500477.
[33] a) C. Zhang, T. Andersson, S. Svensson, O. Björneholm, M. Tchaplyguine, *Phys. Rev. B* **2013**, *87*, 035402; b) K. Dhanabalan, T. Sadhasivam, S. C. Kim, J. J. Eun, J. Shim, D. Jeon, S.-H. Roh, H.-Y. Jung, *J. Mater. Sci. Mater. Electron.* **2017**, *28*, 10349 – 10356.
[34] a) L. Wang, H. Zhou, J. Hu, B. Huang, M. Sun, B. Dong, G. Zheng, Y. Huang, Y. Chen, L. Li, Z. Xu, N. Li, Z. Liu, Q. Chen, L.-D. Sun, C.-H. Yan, *Science* **2019**, *363*, 265 – 270; b) Y. B. Qi, *Sci. Bull.* **2019**, *64*, 224 – 226; c) H. Cho, S.-H. Jeong, M.-H. Park, Y.-H. Kim, C. Wolf, C.-L. Lee, J. H. Heo, A. Sadhanala, N. Myoung, S. Yoo, S. H. Im, R. H. Friend, T.-W. Lee, *Science* **2015**, *350*, 1222 – 1225.
[35] R. G. Wilks, M. Bär, *Nat. Energy* **2017**, *2*, 16204.
[36] N. Liu, C. Yam, *Phys. Chem. Chem. Phys.* **2018**, *20*, 6800 – 6804.
[37] Y. Huang, W.-J. Yin, Y. He, *J. Phys. Chem. C* **2018**, *122*, 1345 – 1350.
[38] J. Kang, L.-W. Wang, *J. Phys. Chem. Lett.* **2017**, *8*, 489 – 493.
[39] S. Yun, X. Zhou, J. Even, A. Hagfeldt, *Angew. Chem. Int. Ed.* **2017**, *56*, 15806 – 15817; *Angew. Chem.* **2017**, *56*, 16014 – 16026.
[40] M. V. Kovalenko, L. Protesescu, M. I. Bodnarchuk, *Science* **2017**, *358*, 745 – 750.
[41] a) S. Heo, G. Seo, Y. Lee, D. Lee, M. Seol, J. Lee, J. B. Park, K. Kim, D. J. Yun, Y. S. Kim, J. K. Shin, T. K. Ahn, M. K. Nazeeruddin, *Energy Environ. Sci.* **2017**, *10*, 1128 – 1133; b) Y. Lin, B. Chen, F. Zhao, X. Zheng, Y. Deng, Y. Shao, Y. Fang, Y. Bai, C. Wang, J. Huang, *Adv. Mater.* **2017**, *29*, 1700607.
[42] a) F. Zu, P. Amsalem, M. Ralaiarisoa, T. Schultz, R. Schlesinger, N. Koch, *ACS Appl. Mater. Interfaces* **2017**, *9*, 41546 – 41552; b) F.-S. Zu, P. Amsalem, I. Salzmann, R.-B. Wang, M. Ralaiarisoa, S. Kowarik, S. Duhm, N. Koch, *Adv. Opt. Mater.* **2017**, *5*, 1700139; c) S. Ravishankar, S. Gharibzadeh, C. Roldán-Carmona, G. Grancini, Y. Lee, M. Ralaiarisoa, A. M. Asiri, N. Koch, J. Bisquert, M. K. Nazeeruddin, *Joule* **2018**, *2*, 788 – 798; d) I. Mora-Seró, *Joule* **2018**, *2*, 585 – 587; e) R. Gottesman, P. Lopez-Varo, L. Gouda, J. A. Jimenez-Tejada, J. Hu, S. Tirosh, A. Zaban, J. Bisquert, *Chem* **2016**, *1*, 776 – 789; f) M. F. Aygüler, A. G. Hufnagel, P. Rieder, M. Wussler, W. Jaegermann, T. Bein, V. Dyakonov, M. L. Petrus, A. Baumann, P. Docampo, *ACS Appl. Mater. Interfaces* **2018**, *10*, 11414 – 11419; g) P. Lopez-Varo, J. A. Jiménez-Tejada, M. García-Rosell, S. Ravishankar, G. Garcia-Belmonte, J. Bisquert, O. Almora, *Adv. Energy Mater.* **2018**, *8*, 1702772; h) J. Bisquert, *The Physics of Solar Cells: Perovskites, Organics, and Photovoltaic Fundamentals*, 1st ed., CRC Press Taylor & Francis Group, Boca Raton, **2018**.
[43] a) G. Gordillo, C. A. Otálora, M. A. Reinoso, *J. Appl. Phys.* **2017**, *122*, 075304; b) J. W. Rosenberg, M. J. Legodi, Y. Rakita, D. Cahen, M. Diale, *J. Appl. Phys.* **2017**, *122*, 145701; c) B. Li, V. Ferguson, S. R. P. Silva, W. Zhang, *Adv. Mater. Interfaces* **2018**, *5*, 1800326; d) V. Adinolfi, M. Yuan, R. Comin, E. S. Thibau, D. Shi, M. I. Saidaminov, P. Kanjanaboos, D. Kopilovic, S. Hoogland, Z.-H. Lu, O. M. Bakr, E. H. Sargent, *Adv. Mater.* **2016**, *28*, 3406 – 3410; e) Y. M. Lee, I. Maeng, J. Park, M. Song, J.-H. Yun, M.-C. Jung, M. Nakamura, *Front. Energy Res.* **2018**, *6*, 128.
[44] O. Hentz, A. Singh, Z. Zhao, S. Gradečak, *Small Methods* **2019**, *3*, 1900110.
[45] I. Levine, O. G. Vera, M. Kulbak, D.-R. Ceratti, C. Rehermann, J. A. Márquez, S. Levcenko, T. Unold, G. Hodes, I. Balberg, D. Cahen, T. Dittrich, *ACS Energy Lett.* **2019**, *4*, 1150 – 1157.
[46] a) Y. Ogomi, K. Kukihara, S. Qing, T. Toyoda, K. Yoshino, S. Pandey, H. Momose, S. Hayase, *ChemPhysChem* **2014**, *15*, 1062 – 1069; b) M. Inaba, J. E. Thorne, D. Wang, W. Y. Sohn, K. Katayama, *J. Photochem. Photobiol. A* **2018**, *364*, 645 – 649; c) T. Leijtens, G. E. Eperon, A. J. Barker, G. Grancini, W. Zhang, J. M. Ball, A. R. S. Kandada, H. J. Snaith, A. Petrozza, *Energy Environ. Sci.* **2016**, *9*, 3472; d) L. M. Herz, *Annu. Rev. Phys. Chem.* **2016**, *67*, 65 – 89; e) V. Adinolfi, W. Peng, G. Walters, O. M. Bakr, E. H. Sargent, *Adv. Mater.* **2017**, *29*, 1700764; f) Y. Yang, M. Yang, D. T. Moore, Y. Yan, E. M. Miller, K. Zhu, M. C. Beard, *Nat. Energy* **2017**, *2*, 16207; g) R. Godin, X. Ma, S. González-Carrero, T. Du, X. Li, C.-T. Lin, M. A. McLachlan, R. E. Galian, J. Pérez-Prieto, J. R. Durrant, *Adv. Opt. Mater.* **2018**, *6*, 1701203; h) J. Shi, Y. Li, Y. Li, D. Li, Y. Luo, H. Wu, Q. Meng, *Joule* **2018**, *2*, 879 – 901.
[47] a) X. Wu, M. T. Trinh, D. Niesner, H. Zhu, Z. Norman, J. S. Owen, O. Yaffe, B. J. Kudisch, X. Y. Zhu, *J. Am. Chem. Soc.* **2015**, *137*, 2089 – 2096; b) M. Kollár, L. Ćirić, J. H. Dil, A. Weber, S. Muff, H. M. Ronnow, B. Náfrádi, B. P. Monnier, J. S. Luterbacher, L. Forró, E. Horváth, *Sci. Rep.* **2017**, *7*, 695; c) M. Yavari, F. Ebadi, S. Meloni, Z. Wang, T. C.-J. Yang, S. Sun, H. Schwartz, Z. Wang, B. Niesen, J. E. Durantini, P. Rieder, K. Tvingstedt, T. Buonassisi, W. C. H. Choy, A. Filippetti, T. Dittrich, S. Olthof, J. P. Correa Baena, W. Tress, *J. Mater. Chem. A* **2019**, *7*, 23838 – 23853; d) P. Schulz, D. Cahen, A. Kahn, *Chem. Rev.* **2019**, *119*, 3349 – 3417.
[48] a) Y. Liu, K. Palotas, X. Yuan, T. Hou, H. Lin, Y. Li, S.-T. Lee, *Acs Nano* **2017**, *11*, 2060 – 2065; b) J. Hieulle, X. Wang, C. Stecker, D.-Y. Son, L. Qiu, R. Ohmann, L. K. Ono, A. Mugarza, Y. Yan, Y. B. Qi, *J. Am. Chem. Soc.* **2019**, *141*, 3515 – 3523; c) L. She, M. Liu, D. Zhong, *Acs Nano* **2016**, *10*, 1126 – 1131; d) A. J. Yost, A. Pimachev, C.-C. Ho, S. B. Darling, L. Wang, W.-F. Su, Y. Dahnovsky, T. Chien, *ACS Appl. Mater. Interfaces* **2016**, *8*, 29110 – 29116; e) M.-C. Shih, S.-S. Li, C.-H. Hsieh, Y.-C. Wang, H.-D. Yang, Y.-P. Chiu, C.-S. Chang, C.-W. Chen, *Nano Lett.* **2017**, *17*, 1154 – 1160; f) L. She, M. Liu, X. Li, Z. Cai, D. Zhong, *Surf. Sci.* **2017**, *656*, 17 – 23; g) L. Cai, L. She, H. Qin, L. Xu, D. Zhong, *Surf. Sci.* **2018**, *675*, 78 – 82.
[49] a) B. Murali, E. Yengel, C. Yang, W. Peng, E. Alarousu, O. M. Bakr, O. F. Mohammed, *ACS Energy Lett.* **2017**, *2*, 846 – 856; b) H.-H. Fang, S. Adjokatse, H. Wei, J. Yang, G. R. Blake, J. Huang, J. Even, M. A. Loi, *Sci. Adv.* **2016**, *2*, e1600534.
[50] a) D.-Y. Son, J.-W. Lee, Y. J. Choi, I.-H. Jang, S. Lee, P. J. Yoo, H. Shin, N. Ahn, M. Choi, D. Kim, N.-G. Park, *Nat. Energy* **2016**, *1*, 16081; b) H. Yu, H. Lu, F. Xie, S. Zhou, N. Zhao, *Adv. Funct. Mater.* **2016**, *26*, 1411 – 1419.
[51] K. P. McKenna, *ACS Energy Lett.* **2018**, *3*, 2663 – 2668.
[52] D. Meggiolaro, E. Mosconi, F. De Angelis, *ACS Energy Lett.* **2017**, *2*, 2794 – 2798.
[53] a) M. Ralaiarisoa, I. Salzmann, F.-S. Zu, N. Koch, *Adv. Electron. Mater.* **2018**, *4*, 1800307; b) M.-A. Stoeckel, M. Gobbi, S. Bonacchi, F. Liscio, L. Ferlauto, E. Orgiu, P. Samorì, *Adv. Mater.* **2017**, *29*, 1702469; c) W. Xu, J. A. McLeod, Y. Yang, Y. Wang, Z. Wu, S. Bai, Z. Yuan, T. Song, Y. Wang, J. Si, R. Wang, X. Gao, X. Zhang, L. Liu, B. Sun, *ACS Appl. Mater. Interfaces* **2016**, *8*, 23181 – 23189.
[54] a) Y. Liu, Z. Yang, D. Cui, X. Ren, J. Sun, X. Liu, J. Zhang, Q. Wei, H. Fan, F. Yu, X. Zhang, C. Zhao, S. Liu, *Adv. Mater.* **2015**, *27*, 5176 – 5183; b) Q. Dong, Y. Fang, Y. Shao, P. Mulligan, J.

Qiu, L. Cao, J. Huang, *Science* **2015**, *347*, 967 – 970; c) M. I. Saidaminov, A. L. Abdelhady, B. Murali, E. Alarousu, V. M. Burlakov, W. Peng, I. Dursun, L. Wang, Y. He, G. Maculan, A. Goriely, T. Wu, O. F. Mohammed, O. M. Bakr, *Nat. Commun.* **2015**, *6*, 7586; d) Z. Lian, Q. Yan, T. Gao, J. Ding, Q. Lv, C. Ning, Q. Li, J.-l. Sun, *J. Am. Chem. Soc.* **2016**, *138*, 9409 – 9412; e) D. Shi, V. Adinolfi, R. Comin, M. Yuan, E. Alarousu, A. Buin, Y. Chen, S. Hoogland, A. Rothenberger, K. Katsiev, Y. Losovyj, X. Zhang, P. A. Dowben, O. F. Mohammed, E. H. Sargent, O. M. Bakr, *Science* **2015**, *347*, 519 – 522; f) Y. Zhang, Y. Liu, Y. Li, Z. Yang, S. Liu, *J. Mater. Chem. C* **2016**, *4*, 9172 – 9178; g) Y. Zhang, Y. Liu, Z. Yang, S. Liu, *J. Energy Chem.* **2018**, *27*, 722 – 727; h) Y. Liu, Y. Zhang, Z. Yang, H. Ye, J. Feng, Z. Xu, X. Zhang, R. Munir, J. Liu, P. Zuo, Q. Li, M. Hu, L. Meng, K. Wang, D.-M. Smilgies, G. Zhao, H. Xu, Z. Yang, A. Amassian, J. Li, K. Zhao, S. Liu, *Nat. Commun.* **2018**, *9*, 5302; i) Y. Zhang, Y. Liu, Z. Xu, H. Ye, Q. Li, M. Hu, Z. Yang, S. Liu, *J. Mater. Chem. C* **2019**, *7*, 1584 – 1591; j) D. Kim, J.-H. Yun, M. Lyu, J. Kim, S. Lim, J. S. Yun, L. Wang, J. Seidel, *J. Phys. Chem. C* **2019**, *123*, 14144 – 14151.

[55] a) Y. Liu, J. Sun, Z. Yang, D. Yang, X. Ren, H. Xu, Z. Yang, S. Liu, *Adv. Opt. Mater.* **2016**, *4*, 1829 – 1837; b) Q. Han, S.-H. Bae, P. Sun, Y.-T. Hsieh, Y. Yang, Y. S. Rim, H. Zhao, Q. Chen, W. Shi, G. Li, Y. Yang, *Adv. Mater.* **2016**, *28*, 2253 – 2258; c) A. A. Zhumekenov, M. I. Saidaminov, M. A. Haque, E. Alarousu, S. P. Sarmah, B. Murali, I. Dursun, X.-H. Miao, A. L. Abdelhady, T. Wu, O. F. Mohammed, O. M. Bakr, *ACS Energy Lett.* **2016**, *1*, 32 – 37; d) J. Pospisil, O. Zmeskal, S. Nespurek, J. Krajcovic, M. Weiter, A. Kovalenko, *Sci. Rep.* **2019**, *9*, 3332.

[56] a) Y. Chen, N. Li, L. Wang, L. Li, Z. Xu, H. Jiao, P. Liu, C. Zhu, H. Zai, M. Sun, W. Zou, S. Zhang, G. Xing, X. Liu, J. Wang, D. Li, B. Huang, Q. Chen, H. Zhou, *Nat. Commun.* **2019**, *10*, 1112; b) S. Ye, H. Rao, Z. Zhao, L. Zhang, H. Bao, W. Sun, Y. Li, F. Gu, J. Wang, Z. Liu, Z. Bian, C. Huang, *J. Am. Chem. Soc.* **2017**, *139*, 7504 – 7512; c) H.-S. Duan, H. Zhou, Q. Chen, P. Sun, S. Luo, T.-B. Song, B. Bob, Y. Yang, *Phys. Chem. Chem. Phys.* **2015**, *17*, 112 – 116.

[57] a) F. Bussolotti, J. Yang, A. Hinderhofer, Y. Huang, W. Chen, S. Kera, A. T. S. Wee, N. Ueno, *Phys. Rev. B* **2014**, *89*, 115319; b) S. Olthof, K. Meerholz, *Sci. Rep.* **2017**, *7*, 40267; c) J. Emara, T. Schnier, N. Pourdavoud, T. Riedl, K. Meerholz, S. Olthof, *Adv. Mater.* **2016**, *28*, 553 – 559.

[58] Y. B. Qi, *Surf. Sci. Rep.* **2011**, *66*, 379 – 393.

[59] a) W. von Ammon, A. Sattler, G. Kissinger, in *Springer Handbook of Electronic and Photonic Materials* (Eds.: S. Kasap, P. Capper), Springer, Cham, **2017**, pp. 112 – 132; b) R. C. Newman, *Rep. Prog. Phys.* **1982**, *45*, 1163 – 1210; c) A. G. Aberle, *Prog. Photovolt. Res. Appl.* **2000**, *8*, 473 – 487.

[60] a) S. H. Lee, M. F. Bhopal, D. W. Lee, S. H. Lee, *Mater. Sci. Semicond. Process.* **2018**, *79*, 66 – 73; b) A. Banerjee, T. Su, D. Beglau, G. Pietka, F. S. Liu, S. Almutawalli, J. Yang, S. Guha, *IEEE J. Photovolt.* **2012**, *2*, 99 – 103; c) A. Banerjee, F. S. Liu, D. Beglau, T. Su, G. Pietka, J. Yang, S. Guha, *IEEE J. Photovolt.* **2012**, *2*, 104 – 108.

[61] Y. Sun, S. Lin, W. Li, S. Cheng, Y. Zhang, Y. Liu, W. Liu, *Engineering* **2017**, *3*, 452 – 459.

[62] a) X. Zheng, B. Chen, J. Dai, Y. Fang, Y. Bai, Y. Lin, H. Wei, X. C. Zeng, J. Huang, *Nat. Energy* **2017**, *2*, 17102; b) S. Yang, J. Dai, Z. Yu, Y. Shao, Y. Zhou, X. Xiao, X. C. Zeng, J. Huang, *J. Am. Chem. Soc.* **2019**, *141*, 5781 – 5787; c) F. Zhang, D. Q. Bi, N. Pellet, C. X. Xiao, Z. Li, J. J. Berry, S. M. Zakeeruddin, K. Zhu, M. Gratzel, *Energy Environ. Sci.* **2018**, *11*, 3480 – 3490.

[63] a) P. Zhao, B. J. Kim, H. S. Jung, *Mater. Today Energy* **2018**, *7*, 267 – 286; b) S. Siebentritt, *Curr. Opin. Green Sustainable Chem.* **2017**, *4*, 1 – 7; c) A. Fakharuddin, F. Di Giacomo, A. L. Palma, F. Matteocci, I. Ahmed, S. Razza, A. D'Epifanio, S. Licoccia, J. Ismail, A. Di Carlo, T. M. Brown, R. Jose, *Acs Nano* **2015**, *9*, 8420 – 8429; d) D. P. Nenon, K. Pressler, J. Kang, B. A. Koscher, J. H. Olshansky, W. T. Osowiecki, M. A. Koc, L.-W. Wang, A. P. Alivisatos, *J. Am. Chem. Soc.* **2018**, *140*, 17760 – 17772; e) C.-C. Chueh, C.-Z. Li, A. K. Y. Jen, *Energy Environ. Sci.* **2015**, *8*, 1160 – 1189; f) F. Wang, S. Bai, W. Tress, A. Hagfeldt, F. Gao, *NPJ Flexible Electron.* **2018**, *2*, 22; g) J. Kim, A. Ho-Baillie, S. Huang, *Solar RRL* **2019**, *3*, 1800302; h) T.-H. Han, S. Tan, J. Xue, L. Meng, J.-W. Lee, Y. Yang, *Adv. Mater.* **2019**, *31*, 1803515; i) H. Zhang, M. K. Nazeeruddin, W. C. H. Choy, *Adv. Mater.* **2019**, *31*, 1805702; j) B. Chen, P. N. Rudd, S. Yang, Y. Yuan, J. Huang, *Chem. Soc. Rev.* **2019**, *48*, 3842 – 3867; k) E. Aydin, M. De Bastiani, S. De Wolf, *Adv. Mater.* **2019**, *31*, 1900428; l) E. M. Tennyson, T. A. S. Doherty, S. D. Stranks, *Nat. Rev. Mater.* **2019**, *4*, 573 – 587.

[64] N. K. Noel, A. Abate, S. D. Stranks, E. S. Parrott, V. M. Burlakov, A. Goriely, H. J. Snaith, *Acs Nano* **2014**, *8*, 9815 – 9821.

[65] A. Abate, M. Saliba, D. J. Hollman, S. D. Stranks, K. Wojciechowski, R. Avolio, G. Grancini, A. Petrozza, H. J. Snaith, *Nano Lett.* **2014**, *14*, 3247 – 3254.

[66] X. Zheng, Y. Deng, B. Chen, H. Wei, X. Xiao, Y. Fang, Y. Lin, Z. Yu, Y. Liu, Q. Wang, J. Huang, *Adv. Mater.* **2018**, *30*, 1803428.

[67] J. Xu, A. Buin, A. H. Ip, W. Li, O. Voznyy, R. Comin, M. Yuan, S. Jeon, Z. Ning, J. J. McDowell, P. Kanjanaboos, J.-P. Sun, X. Lan, L. N. Quan, D. H. Kim, I. G. Hill, P. Maksymovych, E. H. Sargent, *Nat. Commun.* **2015**, *6*, 7081.

[68] a) W. Zhang, S. Pathak, N. Sakai, T. Stergiopoulos, P. K. Nayak, N. K. Noel, A. A. Haghighirad, V. M. Burlakov, D. W. deQuilettes, A. Sadhanala, W. Li, L. Wang, D. S. Ginger, R. H. Friend, H. J. Snaith, *Nat. Commun.* **2015**, *6*, 10030; b) Y. Li, X. Xu, C. Wang, B. Ecker, J. Yang, J. Huang, Y. Gao, *J. Phys. Chem. C* **2017**, *121*, 3904 – 3910.

[69] a) T. Niu, J. Lu, R. Munir, J. Li, D. Barrit, X. Zhang, H. Hu, Z. Yang, A. Amassian, K. Zhao, S. Liu, *Adv. Mater.* **2018**, *30*, 1706576; b) X. Li, M. Ibrahim Dar, C. Yi, J. Luo, M. Tschumi, S. M. Zakeeruddin, M. K. Nazeeruddin, H. Han, M. Grätzel, *Nat. Chem.* **2015**, *7*, 703 – 711.

[70] D. W. de Quilettes, S. M. Vorpahl, S. D. Stranks, H. Nagaoka, G. E. Eperon, M. E. Ziffer, H. J. Snaith, D. S. Ginger, *Science* **2015**, *348*, 683 – 686.

[71] C. Fei, B. Li, R. Zhang, H. Fu, J. Tian, G. Cao, *Adv. Energy Mater.* **2017**, *7*, 1602017.

[72] K. Liu, S. Dai, F. Meng, J. Shi, Y. Li, J. Wu, Q. Meng, X. Zhan, *J. Mater. Chem. A* **2017**, *5*, 21414 – 21421.

[73] F. Meng, K. Liu, S. Dai, J. Shi, H. Zhang, X. Xu, D. Li, X. Zhan, *Mater. Chem. Front.* **2017**, *1*, 1079 – 1086.

[74] M. Zhang, J. Wang, L. Li, G. Zheng, K. Liu, M. Qin, H. Zhou, X. Zhan, *Adv. Sci.* **2017**, *4*, 1700025.

[75] H. Zhu, F. Zhang, Y. Xiao, S. Wang, X. Li, *J. Mater. Chem. A* **2018**, *6*, 4971 – 4980.

[76] G. Yang, P. Qin, G. Fang, G. Li, *Solar RRL* **2018**, *2*, 1800055.

[77] M. Qin, J. Cao, T. Zhang, J. Mai, T.-K. Lau, S. Zhou, Y. Zhou, J. Wang, Y.-J. Hsu, N. Zhao, J. Xu, X. Zhan, X. Lu, *Adv. Energy Mater.* **2018**, *8*, 1703399.

[78] Z. Wu, S. R. Raga, E. J. Juarez-Perez, X. Yao, Y. Jiang, L. K. Ono, Z. Ning, H. Tian, Y. B. Qi, *Adv. Mater.* **2017**, *29*, 1703670.

[79] a) J.-W. Lee, H.-S. Kim, N.-G. Park, *Acc. Chem. Res.* **2016**, *49*, 311 – 319; b) L. Zhu, Y. Xu, P. Zhang, J. Shi, Y. Zhao, H. Zhang, J. Wu, Y. Luo, D. Li, Q. Meng, *J. Mater. Chem. A* **2017**, *5*, 20874 – 20881.

[80] W. Xu, Q. Hu, S. Bai, C. Bao, Y. Miao, Z. Yuan, T. Borzda, A. J. Barker, E. Tyukalova, Z. Hu, M. Kawecki, H. Wang, Z. Yan, X. Liu, X. Shi, K. Uvdal, M. Fahlman, W. Zhang, M. Duchamp, J.-M. Liu, A. Petrozza, J. Wang, L.-M. Liu, W. Huang, F. Gao, *Nat. Photonics* **2019**, *13*, 418 – 424.

[81] D. Wei, F. Ma, R. Wang, S. Dou, P. Cui, H. Huang, J. Ji, E. Jia, X. Jia, S. Sajid, A. M. Elseman, L. Chu, Y. Li, B. Jiang, J. Qiao, Y. Yuan, M. Li, *Adv. Mater.* **2018**, *30*, 1707583.

[82] X. Li, W. Zhang, Y.-C. Wang, W. Zhang, H.-Q. Wang, J. Fang, *Nat. Commun.* **2018**, *9*, 3806.

[83] D. W. deQuilettes, S. Koch, S. Burke, R. K. Paranji, A. J. Shropshire, M. E. Ziffer, D. S. Ginger, *ACS Energy Lett.* **2016**, *1*, 438 – 444.

[84] H. Zhang, Y. Wu, C. Shen, E. Li, C. Yan, W. Zhang, H. Tian, L. Han, W.-H. Zhu, *Adv. Energy Mater.* **2019**, *9*, 1803573.

[85] a) F. Zhang, W. Shi, J. Luo, N. Pellet, C. Yi, X. Li, X. Zhao, T. J. S. Dennis, X. Li, S. Wang, Y. Xiao, S. M. Zakeeruddin, D. Bi, M. Grätzel, *Adv. Mater.* **2017**, *29*, 1606806; b) C.-H. Chiang, C.-G. Wu, *Nat. Photonics* **2016**, *10*, 196 – 200.

[86] K. Wang, C. Liu, P. Du, J. Zheng, X. Gong, *Energy Environ. Sci.* **2015**, *8*, 1245 – 1255.

[87] a) Z. Tang, T. Bessho, F. Awai, T. Kinoshita, M. M. Maitani, R. Jono, T. N. Murakami, H. Wang, T. Kubo, S. Uchida, H. Segawa, *Sci. Rep.* **2017**, *7*, 12183; b) M. Abdi-Jalebi, Z. Andaji-Garmaroudi, S. Cacovich, C. Stavrakas, B. Philippe, J. M. Richter, M. Alsari, E. P. Booker, E. M. Hutter, A. J. Pearson, S. Lilliu, T. J. Savenije, H. Rensmo, G. Divitini, C. Ducati, R. H. Friend, S. D. Stranks, *Nature* **2018**, *555*, 497.

[88] J. Jin, H. Li, C. Chen, B. Zhang, L. Xu, B. Dong, H. Song, Q. Dai, *ACS Appl. Mater. Interfaces* **2017**, *9*, 42875 – 42882.

[89] a) C.-T. Lin, F. De Rossi, J. Kim, J. Baker, J. Ngiam, B. Xu, S. Pont, N. Aristidou, S. A. Haque, T. Watson, M. A. McLachlan, J. R. Durrant, *J. Mater. Chem. A* **2019**, *7*, 3006 – 3011; b) Z. Wang, A. Pradhan, M. A. Kamarudin, M. Pandey, S. S. Pandey, P. Zhang, C. H. Ng, A. S. M. Tripathi, T. Ma, S. Hayase, *ACS Appl. Mater. Interfaces* **2019**, *11*, 10012 – 10020; c) M. Wang, B. Li, J. Yuan, F. Huang, G. Cao, J. Tian, *ACS Appl. Mater. Interfaces* **2018**, *10*, 37005 – 37013; d) W. Gao, K. Zielinski, B. N. Drury, A. D. Carl, R. L. Grimm, *J. Phys. Chem. C* **2018**, *122*, 17882 – 17894; e) W.-Q. Wu, Z. Yang, P. N. Rudd, Y. Shao, X. Dai, H. Wei, J. Zhao, Y. Fang, Q. Wang, Y. Liu, Y. Deng, X. Xiao, Y. Feng, J. Huang, *Sci. Adv.* **2019**, *5*, eaav8925; f) D. Bi, X. Li, J. V. Milić, D. J. Kubicki, N. Pellet, J. Luo, T. LaGrange, P. Mettraux, L. Emsley, S. M. Zakeeruddin, M. Grätzel, *Nat. Commun.* **2018**, *9*, 4482.

[90] a) Z. Chen, B. Turedi, A. Y. Alsalloum, C. Yang, X. Zheng, I. Gereige, A. AlSaggaf, O. F. Mohammed, O. M. Bakr, *ACS Energy Lett.* **2019**, *4*, 1258 – 1259; b) Z. Liu, L. Qiu, E. J. Juarez-Perez, Z. Hawash, T. Kim, Y. Jiang, Z. Wu, S. R. Raga, L. K. Ono, S. Liu, Y. B. Qi, *Nat. Commun.* **2018**, *9*, 3880; c) D. Meggiolaro, E. Mosconi, F. De Angelis, *ACS Energy Lett.* **2019**, *4*, 779 – 785; d) S. D. Stranks, G. E. Eperon, G. Grancini, C. Menelaou, M. J. P. Alcocer, T. Leijtens, L. M. Herz, A. Petrozza, H. J. Snaith, *Science* **2013**, *342*, 341 – 344; e) T. M. Brenner, D. A. Egger, L. Kronik, G. Hodes, D. Cahen, *Nat. Rev. Mater.* **2016**, *1*, 15007.

[91] W. D. Xu, Q. Hu, S. Bai, C. X. Bao, Y. F. Miao, Z. C. Yuan, T. Borzda, A. J. Barker, E. Tyukalova, Z. J. Hu, M. Kawecki, H. Y. Wang, Z. B. Yan, X. J. Liu, X. B. Shi, K. Uvdal, M. Fahlman, W. J. Zhang, M. Duchamp, J. M. Liu, A. Petrozza, J. P. Wang, L. M. Liu, W. Huang, F. Gao, *Nat. Photonics* **2019**, *13*, 418 – 426.

[92] a) Y. Yuan, J. Chae, Y. Shao, Q. Wang, Z. Xiao, A. Centrone, J. Huang, *Adv. Energy Mater.* **2015**, *5*, 1500615; b) K. Domanski, B. Roose, T. Matsui, M. Saliba, S. H. Turren-Cruz, J. P. Correa-Baena, C. R. Carmona, G. Richardson, J. M. Foster, F. De Angelis, J. M. Ball, A. Petrozza, N. Mine, M. K. Nazeeruddin, W. Tress, M. Grätzel, U. Steiner, A. Hagfeldt, A. Abate, *Energy Environ. Sci.* **2017**, *10*, 604 – 613.

[93] a) G. Tong, H. Li, G. Li, T. Zhang, C. Li, L. Yu, J. Xu, Y. Jiang, Y. Shi, K. Chen, *Nano Energy* **2018**, *48*, 536 – 542; b) H. Li, G. Tong, T. Chen, H. Zhu, G. Li, Y. Chang, L. Wang, Y. Jiang, *J. Mater. Chem. A* **2018**, *6*, 14255 – 14261.

[94] a) H. Tan, F. Che, M. Wei, Y. Zhao, M. I. Saidaminov, P. Todorović, D. Broberg, G. Walters, F. Tan, T. Zhuang, B. Sun, Z. Liang, H. Yuan, E. Fron, J. Kim, Z. Yang, O. Voznyy, M. Asta, E. H. Sargent, *Nat. Commun.* **2018**, *9*, 3100; b) M. Saliba, T. Matsui, K. Domanski, J. Y. Seo, A. Ummadisingu, S. M. Zakeeruddin, J. P. Correa-Baena, W. R. Tress, A. Abate, A. Hagfeldt, M. Gratzel, *Science* **2016**, *354*, 206 – 209.

[95] P. Qin, J. Zhang, G. Yang, X. Yu, G. Li, *J. Mater. Chem. A* **2019**, *7*, 1824 – 1834.

[96] T.-H. Han, J.-W. Lee, C. Choi, S. Tan, C. Lee, Y. Zhao, Z. Dai, N. De Marco, S.-J. Lee, S.-H. Bae, Y. Yuan, H. M. Lee, Y. Huang, Y. Yang, *Nat. Commun.* **2019**, *10*, 520.

[97] a) M. Saliba, *Adv. Energy Mater.* **2019**, *9*, 1803754.; b) P. Holzhey, P. Yadav, S.-H. Turren-Cruz, M. Grätzel, A. Hagfeldt, M. Saliba, *Mater. Today* **2018**, *29*, 10 – 19; c) S.-H. Turren-Cruz, A. Hagfeldt, M. Saliba, *Science* **2018**, *362*, 449 – 453.

[98] a) L. K. Ono, E. J. Juárez-Pérez, Y. B. Qi, *ACS Appl. Mater. Interfaces* **2017**, *9*, 30197 – 30246; b) L. K. Ono, Y. B. Qi, S. F. Liu, *Joule* **2018**, *2*, 1961 – 1990.

[99] S. G. Motti, D. Meggiolaro, A. J. Barker, E. Mosconi, C. A. R. Perini, J. M. Ball, M. Gandini, M. Kim, F. De Angelis, A. Petrozza, *Nat. Photon.* **2019**, *13*, 532 – 539.

[100] B. Philippe, T. J. Jacobsson, J.-P. Correa-Baena, N. K. Jena, A. Banerjee, S. Chakraborty, U. B. Cappel, R. Ahuja, A. Hagfeldt, M. Odelius, H. Rensmo, *J. Phys. Chem. C* **2017**, *121*, 26655 – 26666.

[101] Z. Liu, J. Hu, H. Jiao, L. Li, G. Zheng, Y. Chen, Y. Huang, Q. Zhang, C. Shen, Q. Chen, H. Zhou, *Adv. Mater.* **2017**, *29*, 1606774.

[102] a) E. H. Jung, N. J. Jeon, E. Y. Park, C. S. Moon, T. J. Shin, T.-Y. Yang, J. H. Noh, J. Seo, *Nature* **2019**, *567*, 511 – 515; b) L. Han, *Nature* **2019**, *567*, 465 – 467.

[103] J. Peng, J. I. Khan, W. Liu, E. Ugur, T. Duong, Y. Wu, H. Shen, K. Wang, H. Dang, E. Aydin, X. Yang, Y. Wan, K. J. Weber, K. R. Catchpole, F. Laquai, S. De Wolf, T. P. White, *Adv. Energy Mater.* **2018**, *8*, 1801208.

[104] a) Y. Zhao, Q. Li, W. Zhou, Y. Hou, Y. Zhao, R. Fu, D. Yu, X. Liu, Q. Zhao, *Solar RRL* **2019**, *3*, 1800296; b) H. Wang, A. Guerrero, A. Bou, A. M. Al-Mayouf, J. Bisquert, *Energy Environ. Sci.* **2019**, *12*, 2054 – 2079.

[105] a) A. Blakers, *IEEE J. Photovoltaics* **2019**, *9*, 629 – 635; b) A. Wang, J. Zhao, M. A. Green, *Appl. Phys. Lett.* **1990**, *57*, 602 – 604.

[106] a) F. Wang, A. Shimazaki, F. Yang, K. Kanahashi, K. Matsuki, Y. Miyauchi, T. Takenobu, A. Wakamiya, Y. Murata, K. Matsuda, *J. Phys. Chem. C* **2017**, *121*, 1562 – 1568; b) D. Bi, C. Yi, J. Luo, J.-D. Décoppet, F. Zhang, S. M. Zakeeruddin, X. Li, A. Hagfeldt, M. Grätzel, *Nat. Energy* **2016**, *1*, 16142; c) Q. Wang, Q. Dong, T. Li, A. Gruverman, J. Huang, *Adv. Mater.* **2016**, *28*, 6734 – 6739; d) S. Masi, A. Rizzo, F. Aiello, F. Balzano, G. Uccello-Barretta, A. Listorti, G. Gigli, S. Colella, *Nanoscale* **2015**, *7*, 18956 – 18963.

[107] N.-G. Park, H. Segawa, *ACS Photonics* **2018**, *5*, 2970 – 2977.

[108] J. Kim, S. H. Lee, J. H. Lee, K. H. Hong, *J. Phys. Chem. Lett.* **2014**, *5*, 1312 – 1317.

[109] a) Y. Y. Zhou, Y. X. Zhao, *Energy Environ. Sci.* **2019**, *12*, 1495 – 1511; b) E. A. Alharbi, A. Y. Alyamani, D. J. Kubicki, A. R. Uhl, B. J. Walder, A. Q. Alanazi, J. Luo, A. Burgos-Caminal, A. Albadri, H. Albrithen, M. H. Alotaibi, J.-E. Moser, S. M. Zakeeruddin, F. Giordano, L. Emsley, M. Grätzel, *Nat. Commun.* **2019**, *10*, 3008; c) M.-C. Jung, A. Matsuyama, S. Kobori, I. Maeng, Y. M. Lee, M. Song, S.-H. Jin, M. Nakamura, *Sci. Rep.* **2019**, *9*, 10853.

[110] M. R. Leyden, L. Meng, Y. Jiang, L. K. Ono, L. Qiu, E. J. Juarez-Perez, C. Qin, C. Adachi, Y. B. Qi, *J. Phys. Chem. Lett.* **2017**, *8*, 3193 – 3198.

[111] a) J. Ding, Q. Han, Q.-Q. Ge, D.-J. Xue, J.-Y. Ma, B.-Y. Zhao, Y.-X. Chen, J. Liu, D. B. Mitzi, J.-S. Hu, *Joule* **2019**, *3*, 402 – 416; b) J. Li, R. Munir, Y. Fan, T. Niu, Y. Liu, Y. Zhong, Z. Yang, Y. Tian, B. Liu, J. Sun, D.-M. Smilgies, S. Thoroddsen, A. Amassian, K. Zhao, S. Liu, *Joule* **2018**, *2*, 1313 – 1330; c) Y. Jiang, M. Remeika, Z. Hu, E. J. Juarez-Perez, L. Qiu, Z. Liu, T. Kim, L. K. Ono, D.-Y. Son, Z. Hawash, M. R. Leyden, Z. Wu, L. Meng, J. Hu, Y. B. Qi, *Adv. Energy Mater.* **2019**, *9*, 1803047; d) S. R. Raga, Y. Jiang, L. K. Ono, Y. B. Qi, *Energy Technol.* **2017**, *5*, 1750 – 1761; e) S. R. Raga, L. K. Ono, Y. B. Qi, *J. Mater. Chem. A* **2016**, *4*, 2494 – 2500; f) M. Remeika, L. K. Ono, M. Maeda, Z. Hu, Y. B. Qi, *Org. Electron.* **2018**, *54*, 72 – 79; g) M. Remeika, Y. B. Qi, *J. Energy Chem.* **2018**, *27*, 1101 – 1110.

[112] a) L. K. Ono, S. Wang, Y. Kato, S. R. Raga, Y. B. Qi, *Energy Environ. Sci.* **2014**, *7*, 3989 – 3993; b) S. Wang, L. K. Ono, M. R. Leyden, Y. Kato, S. R. Raga, M. V. Lee, Y. B. Qi, *J. Mater. Chem. A* **2015**, *3*, 14631 – 14641; c) M. R. Leyden, L. K. Ono, S. R. Raga, Y. Kato, S. H. Wang, Y. B. Qi, *J. Mater. Chem. A* **2014**, *2*, 18742 – 18745; d) M. R. Leyden, M. V. Lee, S. R. Raga, Y. B. Qi, *J. Mater. Chem. A* **2015**, *3*, 16097 – 16103; e) M. R. Leyden, Y. Jiang, Y. B. Qi, *J. Mater. Chem. A* **2016**, *4*, 13125 – 13132; f) Y. Jiang, M. R. Leyden, L. Qiu, S. Wang, L. K. Ono, Z. Wu, E. J. Juarez-Perez, Y. B. Qi, *Adv. Funct. Mater.* **2018**, *28*, 1703835; g) L. Qiu, S. He, Y. Jiang, D.-Y. Son, L. K. Ono, Z. Liu, T. Kim, T. Bouloumis, S. Kazaoui, Y. B. Qi, *J. Mater. Chem. A* **2019**, *7*, 6920 – 6929; h) L. Qiu, Z. Liu, L. K. Ono, Y. Jiang, D.-Y. Son, Z. Hawash, S. He, Y. B. Qi, *Adv. Funct. Mater.* **2018**, *19*, 1806779; i) L. K. Ono, M. R. Leyden, S. Wang, Y. B. Qi, *J. Mater. Chem. A* **2016**, *4*, 6693 – 6713; j) G. Tong, H. Li, D. Li, Z. Zhu, E. Xu, G. Li, L. Yu, J. Xu, Y. Jiang, *Small* **2018**, *14*, 1702523.

[113] Y. Jiang, E. J. Juarez-Perez, Q. Ge, S. Wang, M. R. Leyden, L. K. Ono, S. R. Raga, J. Hu, Y. B. Qi, *Mater. Horiz.* **2016**, *3*, 548 – 555.

[114] P.-W. Liang, C.-Y. Liao, C.-C. Chueh, F. Zuo, S. T. Williams, X.-K. Xin, J. Lin, A. K. Y. Jen, *Adv. Mater.* **2014**, *26*, 3748 – 3754.

[115] Q. Sun, P. Fassl, Y. Vaynzof, *ACS Appl. Energy Mater.* **2018**, *1*, 2410 – 2416.

[116] a) Z. Chu, M. Yang, P. Schulz, D. Wu, X. Ma, E. Seifert, L. Sun, X. Li, K. Zhu, K. Lai, *Nat. Commun.* **2017**, *8*, 2230; b) Q. Wang, B. Chen, Y. Liu, Y. Deng, Y. Bai, Q. Dong, J. Huang, *Energy Environ. Sci.* **2017**, *10*, 516 – 522; c) Q. Guo, F. Yuan, B. Zhang, S. Zhou, J. Zhang, Y. Bai, L. Fan, T. Hayat, A. Alsaedi, Z. a. Tan, *Nanoscale* **2019**, *11*, 115 – 124.

[117] W.-J. Yin, H. Chen, T. Shi, S.-H. Wei, Y. Yan, *Adv. Electron. Mater.* **2015**, *1*, 1500044.

[118] a) H. Tan, A. Jain, O. Voznyy, X. Lan, F. P. García de Arquer, J. Z. Fan, R. Quintero-Bermudez, M. Yuan, B. Zhang, Y. Zhao, F. Fan, P. Li, L. N. Quan, Y. Zhao, Z.-H. Lu, Z. Yang, S. Hoogland, E. H. Sargent, *Science* **2017**, *355*, 722 – 726; b) L. Qiu, L. K. Ono, Y. Jiang, M. R. Leyden, S. R. Raga, S. Wang, Y. B. Qi, *J. Phys. Chem. B* **2018**, *122*, 511 – 520; c) Y. Ogomi, A. Morita, S. Tsukamoto, T. Saitho, Q. Shen, T. Toyoda, K. Yoshino, S. S. Pandey, T. Ma, S. Hayase, *J. Phys. Chem. C* **2014**, *118*, 16651 – 16659; d) Q. Shen, Y. Ogomi, J. Chang, S. Tsukamoto, K. Kukihara, T. Oshima, N. Osada, K. Yoshino, K. Katayama, T. Toyoda, S. Hayase, *Phys. Chem. Chem. Phys.* **2014**, *16*, 19984 – 19992; e) F. Meng, A. Liu, L. Gao, J. Cao, Y. Yan, N. Wang, M. Fan, G. Wei, T. Ma, *J. Mater. Chem. A* **2019**, *7*, 8690 – 8699.

[119] a) J. Gong, M. Flatken, A. Abate, J.-P. Correa-Baena, I. Mora-Seró, M. Saliba, Y. Zhou, *ACS Energy Lett.* **2019**, *4*, 861 – 865; b) L. K. Ono, T. Kim, Y. Jiang, Y. B. Qi, S. F. Liu, *ACS Energy Lett.* **2018**, *3*, 1898 – 1903; c) L. K. Ono, N.-G. Park, K. Zhu, W. Huang, Y. B. Qi, *ACS Energy Lett.* **2017**, *2*, 1749 – 1751; d) J. Bisquert, Y. B. Qi, T. Ma, Y. Yan, *ACS Energy Lett.* **2017**, *2*, 520 – 523; e) Y. Zhou, K. Zhu, *ACS Energy Lett.* **2016**, *1*, 64 – 67; f) L. Qiu, L. K. Ono, Y. B. Qi, *Mater. Today Energy* **2018**, *7*, 169 – 189.

[120] R. A. Kerner, T. H. Schloemer, P. Schulz, J. J. Berry, J. Schwartz, A. Sellinger, B. P. Rand, *J. Mater. Chem. C* **2019**, *7*, 5251 – 5259.

[121] F. Wang, W. Geng, Y. Zhou, H.-H. Fang, C.-J. Tong, M. A. Loi, L.-M. Liu, N. Zhao, *Adv. Mater.* **2016**, *28*, 9986 – 9992.

[122] Q. Wang, Y. Shao, H. Xie, L. Lyu, X. Liu, Y. Gao, J. Huang, *Appl. Phys. Lett.* **2014**, *105*, 163508.

[123] a) Y. Zong, Y. Zhou, Y. Zhang, Z. Li, L. Zhang, M.-G. Ju, M. Chen, S. Pang, X. C. Zeng, N. P. Padture, *Chem* **2018**, *4*, 1404 – 1415; b) N. Aristidou, I. Sanchez-Molina, T. Chotchuangchutchaval, M. Brown, L. Martinez, T. Rath, S. A. Haque, *Angew. Chem. Int. Ed.* **2015**, *54*, 8208 – 8212; *Angew. Chem.* **2015**, *127*, 8326 – 8330; c) N. Aristidou, C. Eames, I. Sanchez-Molina, X. Bu, J. Kosco, M. S. Islam, S. A. Haque, *Nat. Commun.* **2017**, *8*, 15218.

[124] J.-F. Liao, W.-Q. Wu, J.-X. Zhong, Y. Jiang, L. Wang, D.-B. Kuang, *J. Mater. Chem. A* **2019**, *7*, 9025 – 9033.

[125] a) W. E. I. Sha, X. Ren, L. Chen, W. C. H. Choy, *Appl. Phys. Lett.* **2015**, *106*, 221104; b) C. Wehrenfennig, G. E. Eperon, M. B. Johnston, H. J. Snaith, L. M. Herz, *Adv. Mater.* **2014**, *26*, 1584 – 1589; c) G.-J. A. H. Wetzelaer, M. Scheepers, A. M. Sempere, C. Momblona, J. Ávila, H. J. Bolink, *Adv. Mater.* **2015**, *27*, 1837 – 1841; d) L. M. Pazos-Outón, T. P. Xiao, E. Yablonovitch, *J. Phys. Chem. Lett.* **2018**, *9*, 1703 – 1711.

[126] a) D. Song, P. Cui, T. Wang, D. Wei, M. Li, F. Cao, X. Yue, P. Fu, Y. Li, Y. He, B. Jiang, M. Trevor, *J. Phys. Chem. C* **2015**, *119*, 22812 – 22819; b) P. Cui, D. Wei, J. Ji, H. Huang, E. Jia, S. Dou, T. Wang, W. Wang, M. Li, *Nat. Energy* **2019**, *4*, 150 – 159.

[127] J.-S. Park, A. Walsh, *Nat. Energy* **2019**, *4*, 95 – 96.

[128] D. Meggiolaro, S. G. Motti, E. Mosconi, A. J. Barker, J. Ball, C. A. Riccardo Perini, F. Deschler, A. Petrozza, F. De Angelis, *Energy Environ. Sci.* **2018**, *11*, 702 – 713.

[129] D. B. Khadka, Y. Shirai, M. Yanagida, K. Miyano, *J. Mater. Chem. C* **2018**, *6*, 162 – 170.

[130] a) L. Yucheng, Y. Zhou, L. Shengzhong, *Adv. Sci.* **2018**, *5*, 1700471; b) Y. Liu, Y. Zhang, Z. Yang, D. Yang, X. Ren, L. Pang, S. F. Liu, *Adv. Mater.* **2016**, *28*, 9204 – 9209; c) Y. Liu, X. Ren, J. Zhang, Z. Yang, D. Yang, F. Yu, J. Sun, C. Zhao, Z. Yao, B. Wang, Q. Wei, F. Xiao, H. Fan, H. Deng, L. Deng, S. F. Liu, *Sci. China Chem.* **2017**, *60*, 1367 – 1376; d) Y. Liu, Y. Zhang, K. Zhao, Z. Yang, J. Feng, X. Zhang, K. Wang, L. Meng, H. Ye, M. Liu, S. Liu, *Adv. Mater.* **2018**, *30*, 1707314; e) Y. Liu, Y. Zhang, Z. Yang, J. Feng, X. Zhang, Q. Li, M. Hu, H. Ye, X. Zhang, M. Liu, S. Liu, *Mater. Today* **2019**, *22*, 67 – 75.

[131] Y. Jiang, L. B. Qiu, E. J. Juarez-Perez, L. K. Ono, Z. H. Hu, Z. H. Liu, Z. F. Wu, L. Q. Meng, Q. J. Wang, Y. B. Qi, *Nat. Energy* **2019**, *4*, 585 – 593.

[132] a) A. Zakutayev, C. M. Caskey, A. N. Fioretti, D. S. Ginley, J. Vidal, V. Stevanovic, E. Tea, S. Lany, *J. Phys. Chem. Lett.* **2014**, *5*, 1117 – 1125; b) K. X. Steirer, P. Schulz, G. Teeter, V. Stevanovic, M. Yang, K. Zhu, J. J. Berry, *ACS Energy Lett.* **2016**, *1*, 360 – 366; c) Z. W. Xiao, W. W. Meng, J. B. Wang, D. B. Mitzi, Y. F. Yan, *Mater. Horiz.* **2017**, *4*, 206 – 216; d) R. E. Brandt, V. Stevanović, D. S. Ginley, T. Buonassisi, *MRS Commun.* **2015**, *5*, 265 – 275.

[133] a) D. Cahen, I. Lubomirsky, *Acc. Chem. Res.* **2017**, *50*, 573 – 576; b) D. R. Ceratti, Y. Rakita, L. Cremonesi, R. Tenne, V. Kalchenko, M. Elbaum, D. Oron, M. A. C. Potenza, G. Hodes, D. Cahen, *Adv. Mater.* **2018**, *30*, 1706273; c) Y. Rakita, I. Lubomirsky, D. Cahen, *Mater. Horiz.* **2019**, *6*, 1297 – 1305.

Manuscript received: May 4, 2019
Accepted manuscript online: August 1, 2019
Version of record online: January 29, 2020

